

Closing in on new chiral leptons at the LHC

Daniele Barducci^a, Luca Di Luzio^b, Marco Nardecchia^c, Claudio Toni^{c,d,b}

^a*Dipartimento di Fisica “Enrico Fermi”, Università di Pisa and INFN, Sezione di Pisa,
Largo Bruno Pontecorvo 3, I-56127 Pisa, Italy*

^b*Istituto Nazionale di Fisica Nucleare (INFN), Sezione di Padova,
Via F. Marzolo 8, 35131 Padova, Italy*

^c*Physics Department and INFN Sezione di Roma La Sapienza,
Piazzale Aldo Moro 5, 00185 Roma, Italy*

^d*Dipartimento di Fisica e Astronomia ‘G. Galilei’, Università di Padova,
Via F. Marzolo 8, 35131 Padova, Italy*

We study the phenomenological viability of chiral extensions of the Standard Model, with new chiral fermions acquiring their mass through interactions with a single Higgs. We examine constraints from electroweak precision tests, Higgs physics and direct searches at the LHC. Our analysis indicates that purely chiral scenarios are perturbatively excluded by the combination of Higgs coupling measurements and LHC direct searches. However, allowing for a partial contribution from vector-like masses opens up the parameter space and non-decoupled exotic leptons could account for the observed 2σ deviation in $h \rightarrow Z\gamma$. This scenario will be further tested in the high-luminosity phase of the LHC.

Contents

1	Introduction	2
2	Chiral extensions of the Standard Model	3
3	Phenomenology of new chiral leptons	4
3.1	Electroweak precision tests	4
3.2	Higgs physics	4
3.3	Direct searches	6
3.4	Perturbative unitarity	9
4	Opening up the parameter space with vector-like masses	10
4.1	Numerical analysis	10
4.2	Limit of degenerate masses	11
5	Conclusions	14
A	Other chiral extensions of the Standard Model	14
A.1	Classification with up to four chiral multiplets	15
A.2	Generalization to higher-dimensional $SU(2)_L$ representations	15
B	General formulae for loop-induced Higgs couplings and oblique corrections	16
B.1	General setup	17
B.2	Loop-induced Higgs couplings	18
B.3	Oblique corrections	20

1 Introduction

Before the discovery of the Higgs boson and the accurate determination of its couplings to gauge bosons and third-generation fermions, the possibility of a fourth generation of Standard Model (SM) fermions was a very popular scenario, see *e.g.* [1]. However, due to its non-decoupling nature, purely chiral extensions of the SM imply sizeable modifications in loop-induced Higgs couplings to gluons and photons, so that a fourth generation of SM fermions is nowadays ruled out, at least perturbatively [2–4].

A comprehensive classification of chiral extensions of the SM beyond fourth generation was given in Ref. [5], according to the following requirements: *i*) no massless fermions after electroweak symmetry breaking (EWSB); *ii*) no SM gauge anomalies; *iii*) non-zero corrections to the Higgs boson couplings. Phenomenological viability basically requires the new chiral fermions to be uncolored. In fact, LHC direct searches push the mass of colored states above the TeV and, due to their non-decoupling nature, they in turn modify by $\mathcal{O}(1)$ value the gluon-gluon fusion amplitude for the Higgs production, in stark contradiction with Higgs data. Focussing on uncolored states, hereafter named as exotic leptons, Ref. [5] identified a minimal set of chiral leptons, *cfr.* Eq. (2.1), whose mass stems completely from EWSB and which at that time was still perturbatively viable when considering a combination of phenomenological constraints from electroweak precision tests, Higgs physics and direct searches at the LHC.

Incidentally, the same chiral field content above was invoked in specific ultraviolet (UV) completions of some beyond the SM (BSM) scenarios. In Ref. [6] it was discussed in the context of an axion model featuring axion couplings to electroweak gauge bosons, which were generated after integrating out the heavy chiral leptons charged under a global $U(1)$ symmetry. Another scenario pertains instead the UV completion of a vector boson associated to a $U(1)_X$ gauge symmetry, with X an anomalous combination of the SM global symmetries *e.g.* $B + L$. In this case, the exotic chiral leptons, also charged under $U(1)_X$, are also known as *anomalons*, *i.e.* the fermion sector responsible for the cancellation of gauge anomalies involving $U(1)_X$ and the electroweak gauge factors [7–10]. The role of the anomalons is especially relevant in the case of the effective field theory of a light vector boson coupled to an anomalous SM current since, as argued in Refs. [11, 12], the vector boson interactions feature an axion-like behaviour leading to processes enhanced as $(\text{energy}/m_X)^2$, thus resulting into the typically most stringent bounds on the vector boson parameter space stemming, *e.g.*, from flavour-violating process. In Ref. [13] it was shown that this conclusion relies on the UV completion of the theory and, in particular, the bounds of Refs. [11, 12] are completely evaded if the anomalon fields pick up their mass entirely from the Higgs, that is precisely the phenomenological scenario considered in Ref. [5].

In this work we revisit the phenomenological analysis of Ref. [5], mainly in view of the updated limits from direct searches at the LHC, which have dramatically improved in the last decade. In particular, there are two types of searches which need to be considered, depending on whether the exotic leptons mix or not with the SM leptons. In the former case, they are unstable and strong limits can be obtained by recasting same-sign lepton searches, while in the latter case they are stable, leading to striking signatures at collider, in terms of charged tracks. A further reason to reconsider the scenarios above is given by the recent ATLAS and CMS combination for the search of the $h \rightarrow Z\gamma$ decay channel, whose signal strength is found to be $R_{Z\gamma} = 2.2 \pm 0.7$ [14], thus exhibiting a mild $\sim 2\sigma$ tension with respect to the SM.

The paper is structured as follows. In Sec. 2 we recall the classification of SM chiral extensions of [5], also in light of the new Higgs data. Sec. 3 deals with the phenomenology of purely chiral extensions of the SM, while in Sec. 4 we include the contribution of vector-like components to the masses of the exotic leptons. This allows to open up the parameter space of the model, providing a generalized setup in order to interpret the new $h \rightarrow Z\gamma$ measurement. We finally conclude in Sec. 5, while more technical details on the classification of chiral SM extensions and

general formulae for loop observables are deferred to App. A and App. B, respectively.

2 Chiral extensions of the Standard Model

Purely chiral extensions of the SM are strongly constrained by Higgs couplings measurements. In particular via the loop-induced couplings to gluons and photons, which feature a non-decoupling contribution from heavy chiral fermions acquiring their mass entirely from the Higgs vacuum expectation value (VEV). In this work we assume the presence of a single Higgs doublet, from which all the chiral fermions acquire their mass. However, extended scalar sectors can enlarge the parameter space of Higgs couplings and allow for new chiral fermions with SM-like couplings (see e.g. [15–17]). Given that gluon fusion stands as the predominant mechanism for Higgs production, the introduction of new colored chiral fermions would significantly spoil various Higgs coupling measurements [2–4]. Furthermore, new colored fermions are subject to stringent constraints from direct searches at the LHC which require their mass to be larger than ~ 1 TeV, thus pushing the associated Yukawa couplings with the Higgs beyond the perturbativity regime. Hence, in the following we will focus on color-singlet chiral extensions of the SM with non-trivial electroweak quantum numbers.

The logic for such classification is to find an anomaly-free set of new chiral fermions, whose BSM contribution to $h \rightarrow \gamma\gamma$ interferes with the SM one such that the decay rate is again SM-like. While this classification was discussed in Ref. [5] (see also [18]), we revisit it in App. A also in view of the recent hint for a $h \rightarrow Z\gamma$ signal above the SM value, following the ATLAS and CMS combination which recently measured $R_{Z\gamma} = 2.2 \pm 0.7$ [14]. The bottom-line is that the minimal set of new chiral leptons allowing for a SM-like Higgs coupling to photons is given by [5]

$$\mathcal{L}_{L,R} = \begin{pmatrix} \mathcal{N}_{\mathcal{L}} \\ \mathcal{E}_{\mathcal{L}} \end{pmatrix}_{L,R} \sim (\mathbf{1}, \mathbf{2})_Y, \quad \mathcal{E}_{L,R} \sim (\mathbf{1}, \mathbf{1})_{Y-\frac{1}{2}}, \quad \mathcal{N}_{L,R} \sim (\mathbf{1}, \mathbf{1})_{Y+\frac{1}{2}}, \quad (2.1)$$

which come in opposite chiralities, L and R , in order to cancel SM gauge anomalies.¹ Note that for $Y = -\frac{1}{2}$ the exotic leptons have respectively the same quantum numbers of the SM left-handed doublet L , the right-handed singlet e and a would be right-handed neutrino.

The field content in Eq. (2.1) allows for the following Yukawa interactions with the SM Higgs doublet

$$-\mathcal{L}_y = y_1 \bar{\mathcal{L}}_L H \mathcal{E}_R + y_2 \bar{\mathcal{L}}_R H \mathcal{E}_L + y_3 \bar{\mathcal{L}}_L \tilde{H} \mathcal{N}_R + y_4 \bar{\mathcal{L}}_R \tilde{H} \mathcal{N}_L + h.c., \quad (2.2)$$

where $\tilde{H} = i\sigma_2 H^*$ and σ_2 is the second Pauli matrix. In principle, the SM symmetry would also permit vector-like masses for the new fermions,

$$-\Delta\mathcal{L}_y = m_{\mathcal{L}} \bar{\mathcal{L}}_L \mathcal{L}_R + m_{\mathcal{N}} \bar{\mathcal{N}}_L \mathcal{N}_R + m_{\mathcal{E}} \bar{\mathcal{E}}_L \mathcal{E}_R + h.c., \quad (2.3)$$

which can be forbidden by means of a discrete symmetry or via an extra $U(1)_X$ gauge symmetry that acts differently on the L and R components of the exotic leptons. This latter possibility actually arises in the UV complete models discussed in Ref. [13], where X is an anomalous symmetry of the SM, e.g. $B + L$, and the fields in Eq. (2.1) are introduced in order to cancel the gauge anomalies between $U(1)_X$ and the SM gauge group.

Moreover, for specific values of Y additional Yukawa interactions are possible, allowing for a mixing of the exotic leptons with the SM leptons. Those terms are phenomenologically important and will be discussed in Sec. 3.3.2.

After EWSB the interactions in Eq. (2.2) and Eq. (2.3) produce a spectrum with two 2-flavor Dirac fermions $\Psi^{\mathcal{E}} = (\mathcal{E}_{\mathcal{L}}, \mathcal{E})$ and $\Psi^{\mathcal{N}} = (\mathcal{N}_{\mathcal{L}}, \mathcal{N})$, with electric charge $Q = Y \mp \frac{1}{2}$ respectively.

¹Note that the field content in Eq. (2.1) is formally vector-like under the SM gauge group. In this paper we use the term *chiral* fermion to indicate the absence of a vector-like mass term, which could be forbidden by an extra symmetry beyond that of the SM, *cfr.* discussion below Eq. (2.3).

The mass Lagrangian

$$-\mathcal{L}_{\text{mass}} = \bar{\Psi}_L^{\mathcal{E}} \mathcal{M}_{\mathcal{E}} \Psi_R^{\mathcal{E}} + \bar{\Psi}_L^{\mathcal{N}} \mathcal{M}_{\mathcal{N}} \Psi_R^{\mathcal{N}} + h.c. , \quad (2.4)$$

with mass matrices

$$\mathcal{M}_{\mathcal{E}} = \begin{pmatrix} m_{\mathcal{L}} & \frac{v}{\sqrt{2}} y_1 \\ \frac{v}{\sqrt{2}} y_2^* & m_{\mathcal{E}} \end{pmatrix} , \quad \mathcal{M}_{\mathcal{N}} = \begin{pmatrix} m_{\mathcal{L}} & \frac{v}{\sqrt{2}} y_3 \\ \frac{v}{\sqrt{2}} y_4^* & m_{\mathcal{N}} \end{pmatrix} , \quad (2.5)$$

can be diagonalized by two bi-unitary transformations, yielding the eigenstates $\Psi^{\mathcal{E}_{1,2}}$ and $\Psi^{\mathcal{N}_{1,2}}$ with masses $m_{\Psi^{\mathcal{E}_{1,2}}}$ and $m_{\Psi^{\mathcal{N}_{1,2}}}$ respectively. Note that in the limit $m_{\mathcal{N}} = m_{\mathcal{E}}$, $y_1 = y_3$ and $y_2 = y_4$, hence $\mathcal{M}_{\mathcal{N}} = \mathcal{M}_{\mathcal{E}}$, the Lagrangian sector $\mathcal{L}_y + \Delta\mathcal{L}_y$ features a custodial symmetry which helps in taming corrections to electroweak precision observables.

In the following, we will first discuss in Sec. 3 the phenomenology of purely chiral fermions, *i.e.* the limit of vanishing vector-like masses and then, in Sec. 4, we will analyze the impact of vector-like masses on the parameter space of the model, especially in view of the recent hint of a mild excess in the $h \rightarrow Z\gamma$ decay rate.

3 Phenomenology of new chiral leptons

Among the most relevant phenomenological observables to constrain the parameter space of new chiral leptons, in this section we consider in turn electroweak precision tests, loop-induced Higgs couplings and direct searches, as well as theoretical limits imposed by perturbative unitarity.

3.1 Electroweak precision tests

The new chiral fermions contribute to the Peskin-Takeuchi S and T parameters [19, 20] as [5]

$$\begin{aligned} S &= \frac{1}{6\pi} \left[\left(1 - 2Y \log \frac{m_{\Psi^{\mathcal{N}_1}}^2}{m_{\Psi^{\mathcal{E}_1}}^2} \right) + \left(1 + 2Y \log \frac{m_{\Psi^{\mathcal{N}_2}}^2}{m_{\Psi^{\mathcal{E}_2}}^2} \right) + \mathcal{O} \left(\frac{m_Z^2}{m_{\Psi^{\mathcal{N}, \mathcal{E}}}^2} \right) \right] , \\ T &= \frac{1}{16\pi c_w^2 s_w^2 m_Z^2} \left(m_{\Psi^{\mathcal{N}_1}}^2 + m_{\Psi^{\mathcal{E}_1}}^2 - 2 \frac{m_{\Psi^{\mathcal{N}_1}}^2 m_{\Psi^{\mathcal{E}_1}}^2}{m_{\Psi^{\mathcal{N}_1}}^2 - m_{\Psi^{\mathcal{E}_1}}^2} \log \frac{m_{\Psi^{\mathcal{N}_1}}^2}{m_{\Psi^{\mathcal{E}_1}}^2} \right) \\ &+ \frac{1}{16\pi c_w^2 s_w^2 m_Z^2} \left(m_{\Psi^{\mathcal{N}_2}}^2 + m_{\Psi^{\mathcal{E}_2}}^2 - 2 \frac{m_{\Psi^{\mathcal{N}_2}}^2 m_{\Psi^{\mathcal{E}_2}}^2}{m_{\Psi^{\mathcal{N}_2}}^2 - m_{\Psi^{\mathcal{E}_2}}^2} \log \frac{m_{\Psi^{\mathcal{N}_2}}^2}{m_{\Psi^{\mathcal{E}_2}}^2} \right) . \end{aligned} \quad (3.1)$$

The latest fits for the oblique parameters give [21]: $S = 0.05 \pm 0.11$ and $T = 0.09 \pm 0.13$, which are easily satisfied in the custodial limit $y_1 = y_3$ and $y_2 = y_4$, where $m_{\Psi^{\mathcal{E}_1}} = m_{\Psi^{\mathcal{N}_1}}$ and $m_{\Psi^{\mathcal{E}_2}} = m_{\Psi^{\mathcal{N}_2}}$. Note, also, that contributions beyond S and T , stemming from the loop-induced electroweak corrections to neutral and charged Drell-Yan processes, yield bounds that are weaker than current direct searches (to be discussed in Sec. 3.3), even when considering projections at the high-luminosity phase of LHC (see *e.g.* Ref. [22]).

3.2 Higgs physics

As well known, new fermions which acquire mass from Yukawa interactions with the Higgs field contribute to various Higgs observables. In particular, they modify the predictions for the $h \rightarrow \gamma\gamma$ and $h \rightarrow Z\gamma$ signal strengths, $R_{\gamma\gamma}$ and $R_{Z\gamma}$. These observables are defined as the ratio of the cross-section into the corresponding final state with respect to the SM ones. In the case under consideration of uncolored new states, they can be casted as a ratio of the BSM over the SM branching ratios, which can in turn be expressed in terms of the corresponding squared

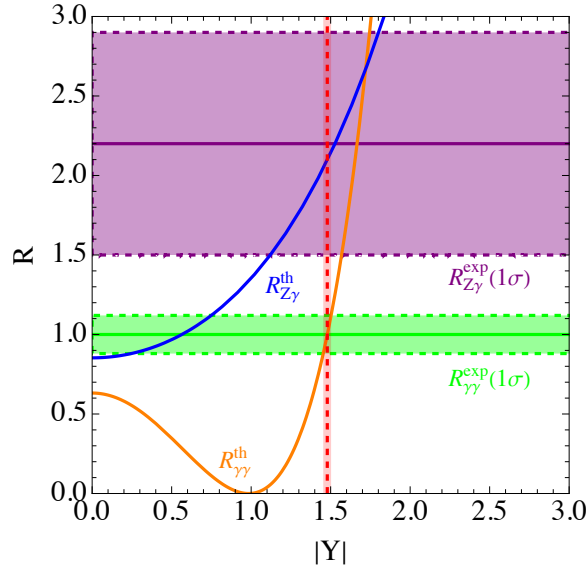


Figure 1: $R_{\gamma\gamma}$ and $R_{Z\gamma}$ signal strengths as a function of the hypercharge Y of the fermion \mathcal{L} . The area between the shaded lines around the central value corresponds to the current 1σ experimental uncertainty.

amplitudes. In particular, by assuming that the new fermions are much heavier than the Higgs boson and with the field content of Eq. (2.1), one has

$$R_{\gamma\gamma, Z\gamma} = \frac{|A_{\gamma\gamma, Z\gamma}^{\text{SM}} + A_{\gamma\gamma, Z\gamma}^{\text{BSM}}|^2}{|A_{\gamma\gamma, Z\gamma}^{\text{SM}}|^2}, \quad (3.2)$$

with $A_{\gamma\gamma}^{\text{SM}} \simeq -6.5$, $A_{Z\gamma}^{\text{SM}} \simeq -6.64$ and

$$\begin{aligned} A_{\gamma\gamma}^{\text{BSM}} &\simeq \frac{4}{3} (1 + 4Y^2), \\ A_{Z\gamma}^{\text{BSM}} &\simeq \frac{2}{3} [1 - (1 + 8Y^2)\text{tg}_w^2], \end{aligned} \quad (3.3)$$

where tg_w is the tangent of the Weinberg angle. The most recent measurement of the $h \rightarrow \gamma\gamma$ signal strength is $R_{\gamma\gamma} = 1.00 \pm 0.12$ [23]. As regarding $h \rightarrow Z\gamma$, the ATLAS and CMS collaboration have recently released a combined measurement which represent the first evidence for this radiative Higgs decay mode. The signal strength is measured to be $R_{Z\gamma} = 2.2 \pm 0.7$ [14]. While the $\gamma\gamma$ mode appear to be in perfect agreement with the SM predictions, the $Z\gamma$ one exhibits a mild $\sim 2\sigma$ tensions.

The predictions of the model with the field content of Eq. (2.1) for these signal strength are shown in Fig. 1 in function of the value Y of the hypercharge for the BSM fermion \mathcal{L} , where the shaded areas around the central values represent the 1σ uncertainty bands. Remarkably, by imposing the model to reproduce the experimental central value for $R_{\gamma\gamma} = 1.00$, one obtains the condition $Y \sim \pm 1.48$, which leads to the prediction $R_{Z\gamma} \sim 2.10$, in notable agreement with the ATLAS and CMS combined measurement [14]. It is also interesting to note that the obtained hypercharge value is close to the semi-integer values $Y = \pm \frac{3}{2}$, which are more theoretically appealing.

Given these constraints, in the following we will thus analyse the phenomenological consequence of the model by fixing $Y \simeq -\frac{3}{2}$, while the case $Y \simeq +\frac{3}{2}$ is simply obtained by charge conjugation.

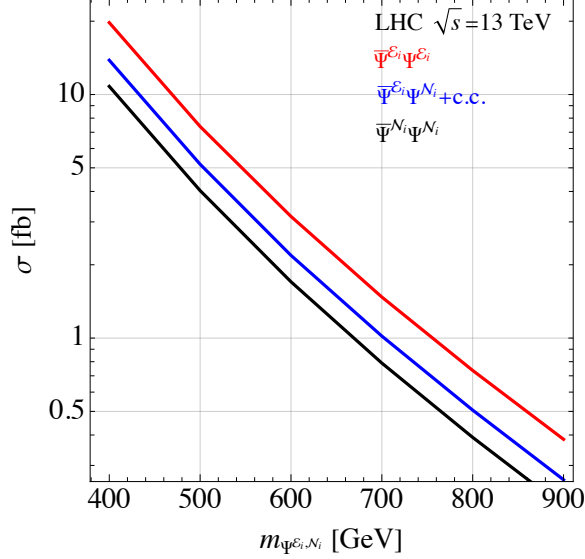


Figure 2: Cross-section for pair-production of a pair of exotic fermions at the 13 TeV LHC. In the case of CC interactions we assume degenerate states $m_{\Psi^{\mathcal{E}_i}} = m_{\Psi^{\mathcal{N}_i}}$.

3.3 Direct searches

With the choice $Y \simeq -\frac{3}{2}$ for the hypercharge of the doublet \mathcal{L} , the two 2-flavor Dirac fermions $\Psi^{\mathcal{E}}$ and $\Psi^{\mathcal{N}}$ have electric charge $Q \simeq -2e$ and $Q \simeq -e$ respectively. At the LHC they can be produced in pair via charged-current (CC) and neutral-current (NC) Drell-Yan (DY) interactions. In the mass eigenbasis their interactions read

$$\begin{aligned} \mathcal{L}_{\text{CC}} &= \frac{g}{\sqrt{2}} \bar{\Psi}^{\mathcal{N}_1} \gamma^\mu P_L \Psi^{\mathcal{E}_1} W_\mu^+ + \frac{g}{\sqrt{2}} \bar{\Psi}^{\mathcal{N}_2} \gamma^\mu P_R \Psi^{\mathcal{E}_2} W_\mu^+ + h.c. , \\ \mathcal{L}_{\text{NC}} &= \frac{g}{c_w} \bar{\Psi}^{\mathcal{E}_i} \gamma^\mu (g_L^{\mathcal{E}_i} P_L + g_R^{\mathcal{E}_i} P_R) \Psi^{\mathcal{E}_i} Z_\mu + \frac{g}{c_w} \bar{\Psi}^{\mathcal{N}_i} \gamma^\mu (g_L^{\mathcal{N}_i} P_L + g_R^{\mathcal{N}_i} P_R) \Psi^{\mathcal{N}_i} Z_\mu , \end{aligned} \quad (3.4)$$

with $P_{L,R} = (1 \mp \gamma_5)/2$ and with

$$\begin{aligned} g_L^{\mathcal{E}_1} = g_R^{\mathcal{E}_2} &= -\frac{1}{2} + 2s_w^2 , & g_R^{\mathcal{E}_1} = g_L^{\mathcal{E}_2} &= 2s_w^2 , \\ g_L^{\mathcal{N}_1} = g_R^{\mathcal{N}_2} &= +\frac{1}{2} + s_w^2 , & g_R^{\mathcal{N}_1} = g_L^{\mathcal{N}_2} &= s_w^2 . \end{aligned} \quad (3.5)$$

We show in Fig. 2 the cross-sections for the production of a pair of new fermions in NC and CC interactions, where in the latter case we assume the custodial limit and the fermions are mass degenerate. The largest rates are the ones for the production of doubly-charged states. As regarding their decay modes, these depends on whether the exotic fermions mix or not with SM fields. We discuss these two scenarios separately.

3.3.1 $Y \neq -\frac{3}{2}$: no mixing with SM leptons

If $Y \neq -\frac{3}{2}$, no mixing terms are allowed. In this case for each flavor i the heaviest between the $\Psi^{\mathcal{E}_i}$ and $\Psi^{\mathcal{N}_i}$ states decays via CC interactions into the lightest one, which is stable because of exotic lepton number conservation. Charged stable states are cosmologically dangerous and largely excluded unless they are not produced in the early Universe or some mechanism dilutes their abundance. They also provide striking signatures at colliders, in terms of charged tracks.

The strongest limit on stable states with $Q = 2e$ is set by the ATLAS analysis [24] which searches for stable particles with various choices for their electric charge, ranging from $Q = 2e$

to $Q = 7e$, and specific coupling structure to the Z -boson. They consider production via both DY and photon-fusion interactions at $\sqrt{s} = 13$ TeV with 139 fb^{-1} of integrated luminosity. By properly taking into account the different coupling structure of the model we are investigating with respect to the one assumed by the ATLAS analysis (see e.g. [25]), one obtains a limit of $m_{\Psi^{\mathcal{E}_i}} \gtrsim 1030$ GeV for a single flavor of doubly charged exotic leptons. This limit increases to ~ 1140 GeV for two degenerate doubly charged exotic leptons.

This analysis does not consider the case of singly charged heavy leptons with $Q = e$. In the scenario where this state is the lightest present in the spectrum, the strongest limit is set by the CMS analysis [26], performed at $\sqrt{s} = 13$ TeV with 3.2 fb^{-1} of integrated luminosity. By recasting the CMS results one obtains a limit $m_{\Psi^{\mathcal{N}_i}} \gtrsim 540$ GeV, with the available data set for a single flavor of singly charged exotic lepton, limits that increases to ~ 630 GeV, for two degenerate singly charged exotic leptons. By projecting the results of this analysis to an integrated luminosity of 139 fb^{-1} , corresponding to the luminosity of the ATLAS search for doubly charged leptons, these limits increase to 820 GeV and 930 GeV respectively.

3.3.2 $Y = -\frac{3}{2}$: exotic fermions mixed with SM leptons

If $Y = -\frac{3}{2}$ additional Yukawa interactions among the exotic and SM leptons are allowed. In particular one has

$$-\mathcal{L}_{\text{mix}} = \lambda_{i,R} \bar{L}_L^i H N_R + \lambda_{i,L} \bar{\mathcal{L}}_L \tilde{H} e_R^i + h.c. , \quad (3.6)$$

which modifies the mass matrix in the $Q = e$ sector. After EWSB we obtain

$$-\mathcal{L}_{\text{mix}} = \frac{v}{\sqrt{2}} \begin{pmatrix} \bar{e}^i \\ \bar{\mathcal{N}}_{\mathcal{L}} \\ \bar{\mathcal{N}} \end{pmatrix}_L \begin{pmatrix} y^{ij} & \lambda_{i,R} & 0 \\ \lambda_{j,L}^T & y_3 & 0 \\ 0 & 0 & y_4^* \end{pmatrix} \begin{pmatrix} e^j \\ \mathcal{N} \\ \mathcal{N}_{\mathcal{L}} \end{pmatrix}_R + h.c. , \quad (3.7)$$

which shows that only one of the exotic $Q = e$ fermions mixes with the SM leptons. Importantly, while the heaviest among $\Psi^{\mathcal{E}_i}$ and $\Psi^{\mathcal{N}_i}$ always decays into the lightest one via CC interactions, this mixing also triggers the decay of the lightest exotic fermions into SM leptons, thus producing a radically different phenomenology with respect to the one of stable charged particles discussed in Sec. 3.3.1. Allowing for the presence of a term like $\mathcal{M}_{\text{mix}}^j \bar{\mathcal{N}}_L e_R^j + h.c.$, produces a mixing among all the $Q = e$ eigenstates, so that for both flavors the lightest state is always unstable. The mixing couplings among anomalous and SM leptons modify the Z couplings to SM charged leptons, which are very well measured, and potentially induce flavour changing violating decays $Z \rightarrow e\mu, \mu\tau, \tau e$. Both the constraints require the mixing angles to be roughly $\lesssim \mathcal{O}(10^{-3})$ and hence their insertion does not modify the calculation of the Higgs signal strength in Eq. (3.3). In a similar way, the CC interactions become

$$\mathcal{L}_{\text{CC}} = \frac{g}{\sqrt{2}} \alpha_i \bar{\Psi}^{\mathcal{E}_1} \gamma^\mu P_L e^i W_\mu^- + \frac{g}{\sqrt{2}} \beta_i \bar{\Psi}^{\mathcal{E}_2} \gamma^\mu P_R e^i W_\mu^- + h.c. , \quad (3.8)$$

where α_i and β_i are mixing angles whose explicit expressions and magnitude are not relevant for the rest of the discussion as long as they are $\gtrsim \mathcal{O}(10^{-7})$, so that doubly charged states promptly decay into a final state with a same-sign (SS) lepton pair via

$$\Psi^{\mathcal{E}_i} \rightarrow W^- \ell^- \rightarrow \ell^- \ell^- \cancel{E}_T . \quad (3.9)$$

Final states with SS leptons have small SM backgrounds. Together with the fact that the DY cross-section for the production of a $\Psi^{\mathcal{E}_i} \bar{\Psi}^{\mathcal{E}_i}$ pair is the largest, see Fig. 2, we expect this process to yield the strongest limit in the scenario where the exotic fermions mix with the SM leptons.

No direct searches for doubly charged leptons exist. There exists however an ATLAS analysis targeting pair-produced doubly charged scalars decaying into a SS lepton pair, performed at $\sqrt{s} = 13$ TeV with 36.1 fb^{-1} of integrated luminosity [27]. In order to recast this analysis we

Signal region	N_{obs}	N_{bkg}	$N_{\text{obs}}^{95\%CL}$	$N_{\text{exp}}^{95\%CL}$
$e^\pm e^\pm$	132	160 ± 14	23.4	39.0
$e^\pm \mu^\pm$	106	97.1 ± 7.7	33.7	27.1
$\mu^\pm \mu^\pm$	26	22.6 ± 2.0	15.1	12.4
$e^\pm e^\pm e^\mp$	11	13.0 ± 1.6	8.1	9.7
$e^\pm \mu^\pm \ell^\mp$	23	34.2 ± 3.6	8.6	16.0
$\mu^\pm \mu^\pm \mu^\mp$	13	13.2 ± 1.3	9.4	10.2
$\ell^\pm \ell^\pm \ell'^\mp$	2	3.1 ± 1.4	4.9	7.0
$\ell^\pm \ell^\pm \ell'^\mp \ell'^\mp$	1	0.33 ± 0.23	4.2	4.2

Table 1: Number of observed events in the various signal region of the ATLAS search [27], together with the SM background expectations. The observed and expected number of excluded signal events are computed via the CLs procedure [31, 32].

have implemented the model into the `Feynrules` [28] package using the `UFO` [29] format in order to perform a simulation with `MadGraph` [30]. The ATLAS search defines 8 mutually exclusive signal regions (SRs), each of them featuring at least one SS lepton pair, categorizing them with respect to lepton multiplicity and flavor.

The basic selection cuts imposed are $p_T^\ell > 30$ GeV, $|\eta_e| < 2.37$ excluding the crack region $1.37 < |\eta_e| < 1.52$ and $|\eta_\mu| < 2.5$. Given that the ATLAS analysis is a simple leptonic cut-and-count search, we decide to work at the parton level, neglecting parton showering and detector reconstruction effects. We expect that the results that we obtain are a good approximation of a more sophisticated procedure. In order to mimic a jet clustering algorithm, needed to apply the lepton/jet overlap removal selections of the analysis, we identify particle level quarks with $p_T^j > 30$ GeV and $|\eta_j| < 5$ as jets. In samples with more than one jet, we merge jets within $\Delta R = 0.4$. Moreover τ leptons are approximated as jets. Further selections are imposed on the kinematics of the event. In all SRs the invariant mass of the SS lepton pairs must be $m_{\ell^\pm \ell^\pm} > 200$ GeV. Furthermore, in regions with more than two leptons events are rejected if any opposite-charge same-flavour lepton pair is within 10 GeV of the Z -boson mass to remove diboson backgrounds. Also, in sample with 2 or 3 leptons it is required $\Delta R(\ell^\pm \ell^\pm) < 3.5$, $p_T^{\ell^\pm \ell^\pm} > 100$ GeV and $\sum |p_T^\ell| > 300$ GeV, where $p_T^{\ell^\pm \ell^\pm}$ is the vector sum of the SS lepton transverse momenta. In the region with four leptons an additional selection is applied. By defining $\bar{M} = \frac{m_{++} + m_{--}}{2}$ and $\Delta M = |m_{++} - m_{--}|$, the analysis requires ΔM values which are below 15 – 50 GeV for $\bar{M} = 200$ GeV, 30 – 160 GeV for $\bar{M} = 500$ GeV, and 50 – 500 GeV for $\bar{M} = 1000$ GeV, depending on the flavor of the leptons.² A summary of the selections is found in Tab. 3 of the ATLAS paper [27]. From the measured number of events in each signal region and the estimation of the SM background we estimate the *observed* number of signal events excluded at 95% confidence level (CL) via the CLs procedure [31, 32]. Projections for higher integrated luminosities are obtained by extrapolating the *expected* 95% CL exclusion. A summary of the exclusion yields are reported in Tab. 1 for the various SRs defined by the ATLAS search.

We then consider the pair-production of both the doubly charged leptons $pp \rightarrow \bar{\Psi}^{\mathcal{E}_{1,2}} \Psi^{\mathcal{E}_{1,2}}$ and study the limits obtained from the recast of the ATLAS search [27], under various assumptions for the flavor mixing pattern of the exotic leptons. For concreteness we study two scenarios. In the former both the exotic fermions only mix with the first two generations of SM leptons with equal weights, thus $\text{BR}(\Psi^{\mathcal{E}_{1,2}} \rightarrow W^- e^-) = \text{BR}(\Psi^{\mathcal{E}_{1,2}} \rightarrow W^- \mu^-) = 50\%$. In the latter we assume them to democratically mix with all the three SM lepton families $\text{BR}(\Psi^{\mathcal{E}_{1,2}} \rightarrow W^- e^-) = \text{BR}(\Psi^{\mathcal{E}_{1,2}} \rightarrow W^- \mu^-) = \text{BR}(\Psi^{\mathcal{E}_{1,2}} \rightarrow W^- \tau^-) = 1/3$. The strongest

²Since ATLAS does not provide any information on the flavor dependence of this cut, we take as cut value the average of the two values and linearly interpolate between different \bar{M} values.

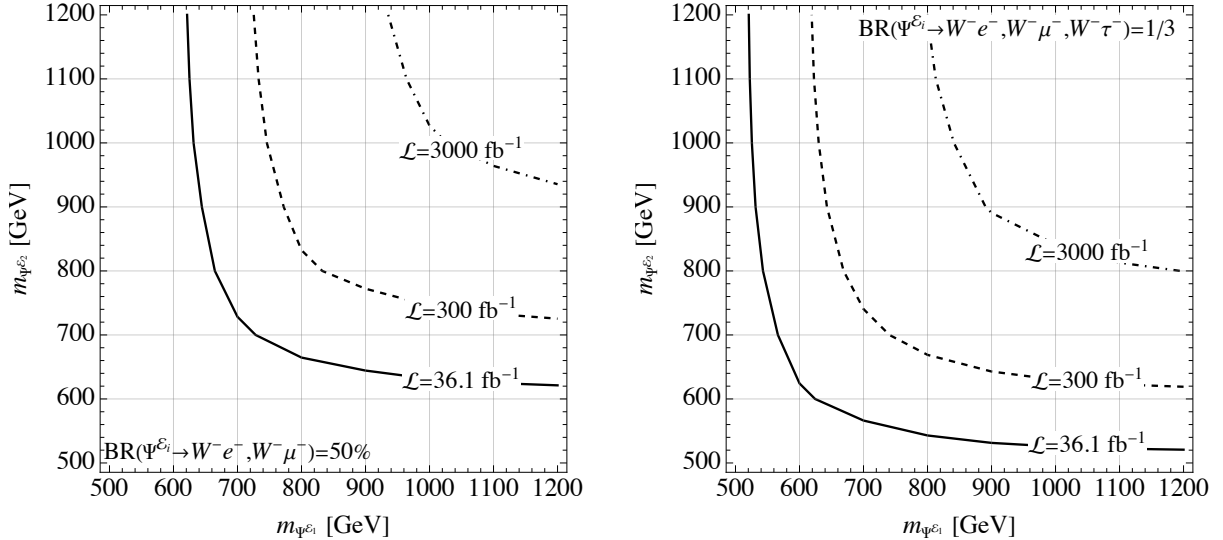


Figure 3: 95% CL exclusion limits obtained from the LHC ATLAS search [27], solid line. The dashed and dot-dashed lines show the projected exclusion with 300 fb^{-1} and 3000 fb^{-1} of integrated luminosity respectively. In the left panel we assume exclusive mixing with the first two generation of SM leptons with equal weights, $\text{BR}(\Psi^{\mathcal{E}_{1,2}} \rightarrow W^- e^-) = \text{BR}(\Psi^{\mathcal{E}_{1,2}} \rightarrow W^- \mu^-) = 50\%$. In the right panel we assume them to democratically mix with all the three SM lepton families $\text{BR}(\Psi^{\mathcal{E}_{1,2}} \rightarrow W^- e^-) = \text{BR}(\Psi^{\mathcal{E}_{1,2}} \rightarrow W^- \mu^-) = \text{BR}(\Psi^{\mathcal{E}_{1,2}} \rightarrow W^- \tau^-) = 1/3$.

exclusion limits come in both cases from SRs with three leptons and are shown in Fig. 3 for the actual luminosity of the ATLAS search, $\mathcal{L} = 36.1 \text{ fb}^{-1}$, as well as for two projected benchmark values, $\mathcal{L} = 300, 3000 \text{ fb}^{-1}$. Current limits in the first scenario are around 600 GeV, if one of the two exotic lepton is decoupled from the spectrum, reaching ~ 720 GeV if the two states are mass degenerate. At the end of the high-luminosity phase of the LHC, values up to $m_{\Psi^{\mathcal{E}_{1,2}}} \simeq 1 \text{ TeV}$ could be tested. Allowing for a mixing with the τ lepton, relaxes these limits of $\mathcal{O}(100 \text{ GeV})$ given that this final state is not directly targeted by the analysis [27], and is anyway expected to be harder to be tested.

Turning our attention to the $Q = e$ exotic states, they promptly decay, for mixing angles $\gtrsim \mathcal{O}(10^{-7})$, as

$$\Psi^{\mathcal{N}_i} \rightarrow W^- \nu, Z \ell^- , \quad (3.10)$$

where the branching ratio of each channel is a function of the model parameters. The experimental signature depends on how the W or Z bosons decay and, in particular, signatures as in Tab. 1 are possible. The inclusion of the $\Psi^{\mathcal{N}_i}$ decay modes would then increase the constraints from direct searches, but it requires a less straightforward analysis than the one performed for the double charged states. We choose to be conservative and rely on the constraints we already obtained in Fig. 3 since the take-home message of this work, which is that purely chiral extensions of the SM lie beyond the edge of perturbativity, as we will discuss in the next section, would not substantially change.

3.4 Perturbative unitarity

In Sec. 3.3.2 we have shown that current LHC limits push the exotic leptons to have a mass $\gtrsim 500 - 600 \text{ GeV}$, depending on the flavor structure of the model, in the case that they mix with the SM fermions. In case of no SM-BSM mixing these limits are pushed to even higher values, from the null results for searches of heavy-stable charged particles, see Sec. 3.3.1.

If the exotic fermions are chiral states which acquire their mass only via their couplings to the Higgs, the Yukawa couplings $y_{1,2}$ and $y_{3,4}$ attain large values, possibly at the edge of the per-

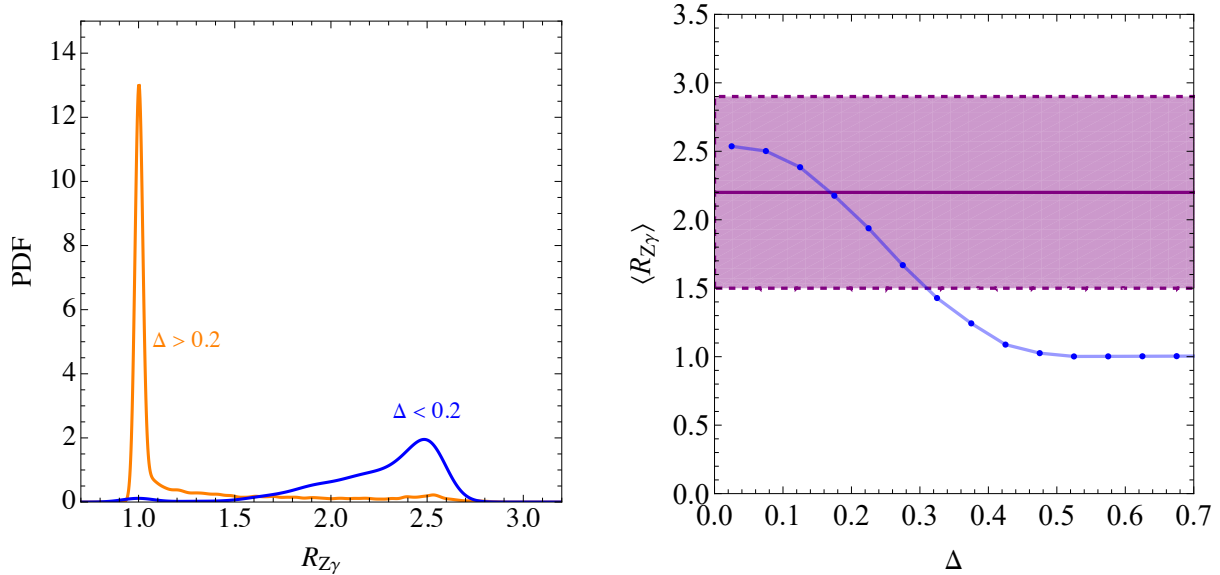


Figure 4: *Left panel:* Distribution of the $R_{Z\gamma}$ predictions for two regions of the mass-splitting parameters: $\Delta < 0.2$ and $\Delta > 0.2$. *Right panel:* Average value of the $R_{Z\gamma}$ predictions as function of the mass-splitting parameter Δ .

turbative regime. In order to quantify this statement we apply the procedure discussed in [33], see also [34], and compute the perturbative unitarity (PU) bounds obtained by considering all the $2 \rightarrow 2$ scatterings present in the model. The strongest limit is obtained in the $J = 0$ partial wave and, working for simplicity in the custodial limit $y_1 = y_3$, $y_2 = y_4$, reads

$$3|y_1|^2 + 3|y_2|^2 + \sqrt{9|y_2|^4 - 2|y_1|^2|y_2|^2 + 9|y_2|^4} < 16\pi . \quad (3.11)$$

This bound can be then translated into a perturbative *upper limit* on the exotic fermion masses, which fixes $m_{\Psi^{\varepsilon_{1,2}}} \lesssim 400$ GeV. Hence, current LHC limits perturbatively exclude the model, according to the criterium in Eq. (3.11).

4 Opening up the parameter space with vector-like masses

We have seen that SM extensions with exotic chiral fermions are pushed beyond the edge of their perturbativity regime by direct searches. In this section we thus consider the effect of the addition of vector-like masses, in order to avoid the constraints from direct searches while being compatible with the electroweak precision test and the recent measurement of $h \rightarrow Z\gamma$.

4.1 Numerical analysis

Since we were not able in general to cast explicit expressions for the $h \rightarrow \gamma\gamma$, $Z\gamma$ theoretical predictions and for the Peskin-Takeuchi parameters into a simple analytical form, see Eqs. (B.18)–(B.21) and Eqs. (B.28)–(B.29), we rely on a numerical analysis to study the $R_{Z\gamma}$ prediction when the vector-like masses are included. In particular, we randomly scan the parameters of the Lagrangian in Eq. (2.2) and Eq. (2.3) within the intervals³

$$|m_{\mathcal{L}, \mathcal{N}, \varepsilon}| \in [1.7, 2] \text{ TeV} \quad \text{and} \quad |y_{1,2,3,4}| \in \left[1, \sqrt{\frac{8\pi}{5}}\right], \quad (4.1)$$

³The parameters that allows mixing along exotic and SM leptons are highly constrained by precise measurements of the Z coupling and hence are negligible in all the practical calculations.

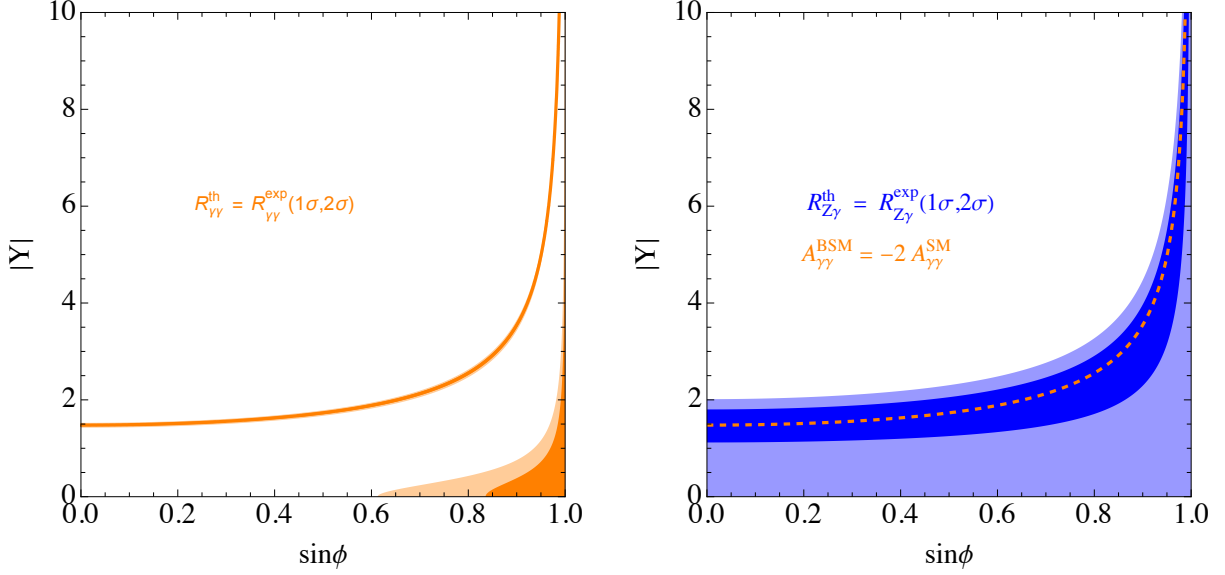


Figure 5: *Left panel:* Allowed region of $R_{\gamma\gamma}$ at 1σ and 2σ in the $\sin\phi - |Y|$ plane. *Right panel:* Allowed region of $R_{Z\gamma}$ at 1σ and 2σ in the $\sin\phi - |Y|$ plane. The dashed yellow line indicates the non-decoupling solution $A_{\gamma\gamma}^{\text{BSM}} \simeq -2A_{\gamma\gamma}^{\text{SM}}$.

so that the PU bound on the Yukawa couplings is always satisfied. For each point extracted, the value of the hypercharge parameter Y is set by minimizing the χ^2 of the S and $R_{\gamma\gamma}$ observables⁴

$$\chi^2 = \left(\frac{R_{\gamma\gamma} - \mu_{\gamma\gamma}}{\sigma_{\gamma\gamma}} \right)^2 + \left(\frac{S - \mu_S}{\sigma_S} \right)^2, \quad (4.2)$$

where $\mu_{\gamma\gamma} = 1.00$, $\sigma_{\gamma\gamma} = 0.12$, $\mu_S = 0.05$, $\sigma_S = 0.11$. Finally we evaluate the theoretical prediction of the $h \rightarrow Z\gamma$ channel for each point and plot the results in Fig. 4, where the parameter

$$\Delta \equiv \left| \frac{m_{\Psi}^2 \varepsilon_1 - m_{\Psi}^2 \varepsilon_2}{m_{\Psi}^2 \varepsilon_1 + m_{\Psi}^2 \varepsilon_2} \right| + \left| \frac{m_{\Psi}^2 \mathcal{N}_1 - m_{\Psi}^2 \mathcal{N}_2}{m_{\Psi}^2 \mathcal{N}_1 + m_{\Psi}^2 \mathcal{N}_2} \right| \quad (4.3)$$

measures the degeneracy of the \mathcal{E} and \mathcal{N} exotic states. As we can see from the plots, the inclusion of vector-like mass terms would generally lead to $R_{Z\gamma}$ values around unity, *i.e.* SM-like, unless the exotic leptons are degenerate, in which case the $h \rightarrow Z\gamma$ prediction lies within the 1σ region of the ATLAS and CMS combined measurement.

4.2 Limit of degenerate masses

As shown above, the $h \rightarrow Z\gamma$ prediction naturally lies in the 1σ region of the ATLAS and CMS measurement in the limit of mostly degenerate masses, *i.e.* $\Delta \rightarrow 0$. Motivated by this result, we now specify our study to the case of fully degenerate exotic masses, that is

$$\mathcal{M}_{\mathcal{E}}^\dagger \mathcal{M}_{\mathcal{E}} = \mathcal{M}_{\mathcal{N}}^\dagger \mathcal{M}_{\mathcal{N}} = m_{\Psi}^2 \begin{pmatrix} 1 & 0 \\ 0 & 1 \end{pmatrix}, \quad (4.4)$$

with m_{Ψ} denoting the common mass value. Eq. (4.4) enforces the mass matrices to be

$$\mathcal{M}_{\mathcal{E}} = \mathcal{M}_{\mathcal{N}} = \begin{pmatrix} M & \pm i \frac{v}{\sqrt{2}} y_H \\ \pm i \frac{v}{\sqrt{2}} y_H & M \end{pmatrix} = m_{\Psi} \begin{pmatrix} \sin\phi & \pm i \cos\phi \\ \pm i \cos\phi & \sin\phi \end{pmatrix}, \quad (4.5)$$

⁴The observable T is independent of the hypercharge Y and hence it is not considered in the χ^2 analysis.

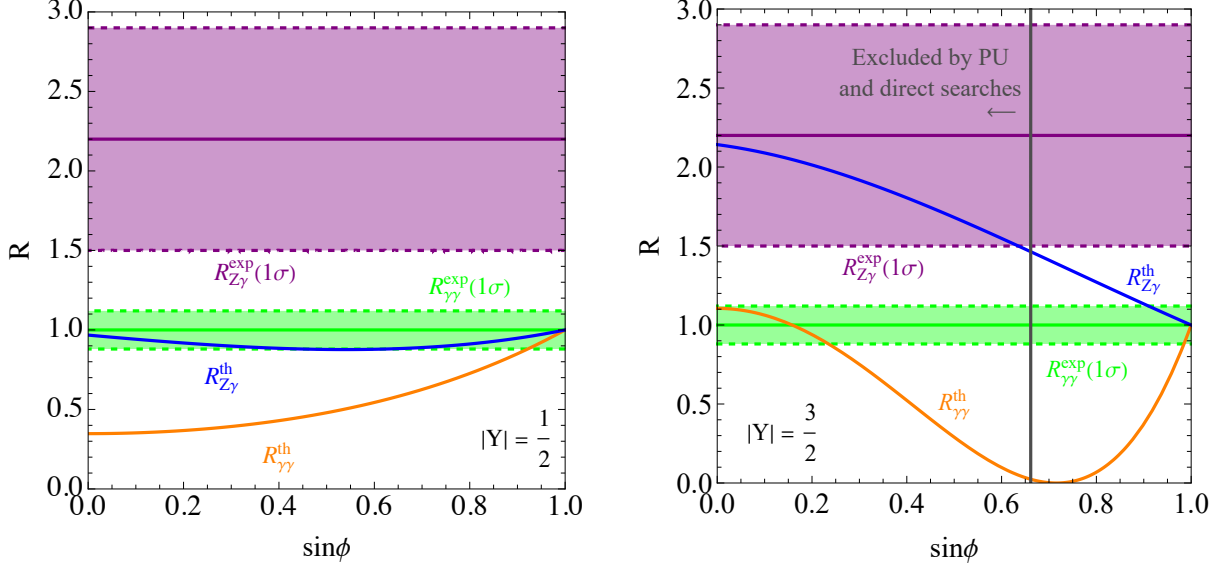


Figure 6: $R_{\gamma\gamma}$ and $R_{Z\gamma}$ signal strengths as a function of $\sin\phi$ for $|Y| = 1/2$ (left panel) and $\sin\phi$ for $|Y| = 3/2$ (right panel). The area between the shaded lines around the central value corresponds to the current 1σ experimental uncertainty. The region on the left of the gray line is excluded by the PU and direct search constraints discussed in Sec. 3.3.1.

with y_H, M real and positive parameters, while the physical mass reads

$$m_\Psi^2 = M^2 + \frac{1}{2}(y_H v)^2 \quad (4.6)$$

and

$$\cos\phi = \frac{1}{\sqrt{2}} \frac{y_H v}{m_\Psi}, \quad (4.7)$$

is the cosine of the angle measuring the relative contribution of the chiral mass on the total one.

The PU constraint Eq. (3.11) enforces on the degenerate case the bound $y_H^2 < 8\pi/5$. In the degenerate limit the Peskin-Takeuchi parameter T is zero due to the custodial symmetry while

$$S \simeq \frac{1}{3\pi} \cos^2\phi, \quad (4.8)$$

which is always compatible with the experimental constraint for every value of the cosine. Furthermore, the insertion of vector-like masses in the degenerate limit modifies Eq. (3.3) as

$$\begin{aligned} A_{\gamma\gamma}^{\text{BSM}} &\simeq \frac{4}{3} (1 + 4Y^2) \cos^2\phi, \\ A_{Z\gamma}^{\text{BSM}} &\simeq \frac{2}{3} [1 - (1 + 8Y^2) \text{tg}_w^2] \cos^2\phi, \end{aligned} \quad (4.9)$$

so that $R_{\gamma\gamma, Z\gamma}$ depend on two parameters, the hypercharge Y and mixing angle ϕ . In Fig. 5 we show the 1σ , dark shaded, and 2σ , light shaded, allowed regions of the $R_{\gamma\gamma, Z\gamma}$ observables in the $\sin\phi - |Y|$ plane. Note that the $R_{\gamma\gamma}$ plot shows two different allowed regions, relative to the two SM-like solutions: the decoupling scenario $A_{\gamma\gamma}^{\text{BSM}} \simeq 0$ in the bottom right corner of the figure and the non-decoupling one $A_{\gamma\gamma}^{\text{BSM}} \simeq -2A_{\gamma\gamma}^{\text{SM}}$. Different considerations on these solutions then apply depending on if the exotic leptons are stable or unstable.

4.2.1 Unstable exotic leptons

Exotic leptons can mix with the SM fields, and hence decay into SM states, only for $|Y| = \frac{1}{2}, \frac{3}{2}$. We plot in Fig. 6 the $h \rightarrow \gamma\gamma, Z\gamma$ predictions for these two hypercharge values as a function of

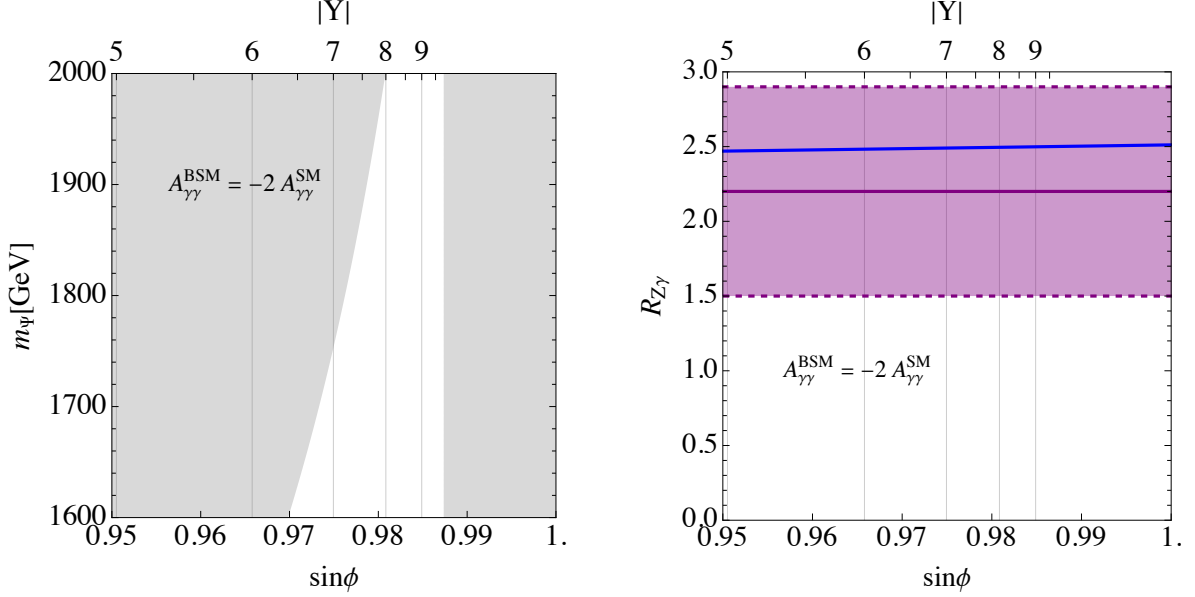


Figure 7: *Left panel:* Exclusion region due to PU bounds and direct searches constraints in the $\sin\phi - m_\Psi$ plane. *Right panel:* $R_{Z\gamma}$ as a function of $\sin\phi$. In both panel the corresponding value of Y is also shown and the non-decoupling solution $A_{\gamma\gamma}^{\text{BSM}} = -2A_{\gamma\gamma}^{\text{SM}}$ is imposed.

$\sin\phi$. For $|Y| = 1/2$ we observe on left panel that the $h \rightarrow \gamma\gamma$ prediction is compatible with the experimental value only in the decoupling region where $R_{\gamma\gamma, Z\gamma} \approx 1$. A similar conclusion holds for $|Y| = 3/2$, where we observe on the right panel that the PU bound on the Yukawa couplings and the direct search constraints discussed in Sec. 3.3.1 exclude the $A_{\gamma\gamma}^{\text{BSM}} \approx -2A_{\gamma\gamma}^{\text{SM}}$ solution, leading again to a scenario with decoupled exotic leptons. In either of the two cases above, it is then trivially possible in the decoupling regime to be compatible with the SM prediction $R_{\gamma\gamma, Z\gamma} \approx 1$. However, it is not possible to explain the 2σ hint for $h \rightarrow Z\gamma$.

4.2.2 Stable exotic leptons

For $|Y| \neq 1/2, 3/2$ mixing terms with the SM fermions are forbidden and the exotic leptons are stable, hence direct searches constrain the exotic mass to be $\gtrsim 1600$ GeV as already discussed in Sec. 3.3.1. Such strong constraint leads to a mostly-decoupled scenario where vector-like masses must dominate over the chiral contribution. Hence in order to obtain values of $R_{Z\gamma}$ different from unity, large values of the hypercharge Y are required. Along with the one on the Yukawa couplings, a PU bound on the hypercharge Y can be computed with the procedure discussed in Ref. [35] by considering the $\psi B \rightarrow \psi B$ scattering⁵, where B is the hypercharge field and ψ the exotic lepton field. The strongest limit is obtained in the $J = 1/2$ partial wave and reads

$$\text{Max} \left\{ Y^2, \left(Y + \frac{1}{2} \right)^2, \left(Y - \frac{1}{2} \right)^2 \right\} < \frac{4\pi}{g_Y^2}, \quad (4.10)$$

which yields $|Y| \lesssim 10$ for $g_Y = 0.36$. In the left panel of Fig. 7 we show the exclusion region due to the PU bounds on the Yukawa couplings and the hypercharge Y as a function of the degenerate mass m_Ψ and the lower limit enforced by LHC direct searches, while imposing the non-decoupling solution $A_{\gamma\gamma}^{\text{BSM}} = -2A_{\gamma\gamma}^{\text{SM}}$. In the region allowed by PU and direct search constraints, the $R_{Z\gamma}$ prediction is around ~ 2.5 as shown in the right panel of Fig. 7.

⁵This is the only $2 \rightarrow 2$ scattering channel with non-singular partial amplitude when the vector field is taken to be exactly massless in the high-energy limit.

In the near future the HL-LHC is expected to measure the $h \rightarrow Z\gamma$ decay within 10% precision [36]. In particular ATLAS plans to reduce the uncertainty from the present value ± 0.9 [14] down to ± 0.23 [36], hence to improve it by a factor of $\sim 25\%$. By considering that the same improvement will be obtained for the uncertainty of a combined ATLAS and CMS analysis and assuming that the present central value will not change with future measurements, one will obtain $R_{Z\gamma}^{\text{HL-LHC}} = 2.2 \pm 0.2$, that is a measured value which is more than 5σ away from the SM value. In such a, highly speculative, case one would need some non-decoupling new physics, like the one discussed in the present work, in order to keep $R_{\gamma\gamma}$ SM-like and explain at the same time a non-standard value of $R_{Z\gamma}$.

5 Conclusions

In this work we presented a detailed exploration of the phenomenology associated with chiral extensions to the SM coupled to a single Higgs doublet, particularly focussing on exotic leptons. Our study revisits and expands upon the original analysis provided in Ref. [5], incorporating the latest data from LHC direct searches. These insights have been crucial in delineating the parameter space for these chiral extensions, especially in light of the stringent constraints imposed by recent experimental results.

Our findings highlight that purely chiral scenarios are perturbatively ruled out when considering the combined constraints from Higgs coupling measurements and direct LHC searches. On the other hand, by incorporating vector-like mass components into the exotic leptons, we observe an intriguing expansion of the viable parameter space. This extended framework not only aligns with the current 2σ deviation observed in the $h \rightarrow Z\gamma$ channel but also provides a fertile ground for future experimental investigations, particularly with the upcoming high-luminosity phase of the LHC.

As a by-product of our analysis we also conclude that the possibility pointed out in Ref. [13] to avoid the strong constraints stemming from the coupling of light vector bosons to anomalous SM currents [11, 12], is not anymore viable, at least perturbatively, since it relies on the hypothesis of purely chiral anomalon fields.

Acknowledgments

We thank Michele Frigerio for useful discussions. The work of LDL, MN and CT is supported by the by the Italian Ministry of University and Research (MUR) via the PRIN 2022 project n. 2022K4B58X – AxionOrigins. The work of LDL is also supported by the European Union – NextGenerationEU and by the University of Padua under the 2021 STARS Grants@Unipd programme (Acronym and title of the project: CPV-Axion – Discovering the CP-violating axion), the European Union’s Horizon 2020 research and innovation programme under the Marie Skłodowska-Curie grant agreement n. 101086085 – ASYMMETRY and the INFN Iniziative Specifica APINE.

A Other chiral extensions of the Standard Model

In this Appendix we consider more general chiral extensions of the SM, other than the one of Eq. (2.1), and show that they do not allow to reproduce a value of $R_{Z\gamma}$ compatible with the current experimental limits, thus supporting the choice of the field content studied in the main text.

A.1 Classification with up to four chiral multiplets

Let us consider fermionic extensions of the SM given by an anomaly-free set of up to four chiral multiplets, as discussed in [5]. We require that no vector-like mass terms are allowed, no exotic state is left massless after EWSB and that each field is a singlet under QCD. These requirements leave us with only one possible set, composed by four chiral BSM fermions transforming under the SM as [5]

$$\chi_{2R} \sim (\mathbf{1}, \mathbf{2I+2})_0, \quad \psi_{1R} \sim (\mathbf{1}, \mathbf{2I+1})_{-\frac{1}{2}}, \quad \psi_{2R} \sim (\mathbf{1}, \mathbf{2I+1})_{+\frac{1}{2}}, \quad \chi_{1R} \sim (\mathbf{1}, \mathbf{2I})_0, \quad (\text{A.1})$$

with the isospin quantum number I being necessarily a semi-integer to avoid the global $SU(2)_L$ anomaly [37]. All the fields can take mass from the SM Higgs through the Yukawa Lagrangian

$$-\mathcal{L}_{\text{Yukawa}} = y_{21} \overline{(\psi_{2R})^c} \tilde{H} \chi_{1R} + y_{22} \overline{(\psi_{2R})^c} \tilde{H} \chi_{2R} + y_{11} \overline{(\chi_{1R})^c} H \psi_{1R} + y_{12} \overline{(\chi_{2R})^c} H \psi_{1R} + h.c., \quad (\text{A.2})$$

where isospin contractions are left implicit. The Lagrangian of Eq. (A.2) admits the global symmetry

$$U(1)_R: \quad \chi_{iR} \rightarrow e^{i\theta} \chi_{iR}, \quad \psi_{iR} \rightarrow e^{-i\theta} \psi_{iR} \quad i = 1, 2, \quad (\text{A.3})$$

that can prevent any additional Yukawa or mass term that involves the exotic fields. Assuming the exotic fermions to be much heavier than the Higgs and Z bosons after EWSB, one gets the following BSM contribution to $h \rightarrow \gamma\gamma, Z\gamma$ decay

$$A_{\gamma\gamma}^{\text{BSM}} \simeq \frac{4}{9} (2I+1)(3+4I+4I^2), \quad (\text{A.4})$$

$$A_{Z\gamma}^{\text{BSM}} \simeq \frac{1+2I}{9} [3+8I+8I^2 - \text{tg}_w^2(9+8I+8I^2)]. \quad (\text{A.5})$$

In Tab. 2 we report the $R_{\gamma\gamma, Z\gamma}$ predictions for the lowest values of the isospin I . As one can note, we are never able to reproduce the experimental results for any value of I .

	$I = \frac{1}{2}$	$I = \frac{3}{2}$	$I = \frac{5}{2}$
$R_{\gamma\gamma}$	~ 0.03	~ 15	~ 213
$R_{Z\gamma}$	~ 0.7	~ 0.3	~ 19

Table 2: $R_{\gamma\gamma, Z\gamma}$ predictions for the lowest values of the isospin I .

A.2 Generalization to higher-dimensional $SU(2)_L$ representations

We next explore a generalization of the field content described in Eq. (2.1) with arbitrary $SU(2)_L$ representations. In particular, we consider BSM fermions vector-like under the SM, with respect to which they transform as

$$\mathcal{L} \sim (\mathbf{1}, \mathbf{2I+1})_Y, \quad \mathcal{E} \sim (\mathbf{1}, \mathbf{2I})_{Y-\frac{1}{2}}, \quad \mathcal{N} \sim (\mathbf{1}, \mathbf{2I})_{Y+\frac{1}{2}}, \quad \mathcal{F} \sim (\mathbf{1}, \mathbf{2I-1})_Y, \quad (\text{A.6})$$

where I is the isospin of the largest $SU(2)_L$ representation, whose value is restricted to integer or semi-integer values. Note that for $I = 1/2$ the \mathcal{F} field is absent and we are left with the same field content as Eq. (2.1). All the fields can take mass from the SM Higgs through the Yukawa Lagrangian

$$-\mathcal{L}_{\text{Yukawa}} = y_{R1} \overline{\mathcal{L}}_L \tilde{H} \mathcal{N}_R + y_{L1} \overline{\mathcal{L}}_R \tilde{H} \mathcal{N}_L + y_{R2} \overline{\mathcal{F}}_L \tilde{H} \mathcal{N}_R + y_{L2} \overline{\mathcal{F}}_R \tilde{H} \mathcal{N}_L + y_{R3} \overline{\mathcal{L}}_L H \mathcal{E}_R + y_{L3} \overline{\mathcal{L}}_R H \mathcal{E}_L + y_{R4} \overline{\mathcal{F}}_L H \mathcal{E}_R + y_{L4} \overline{\mathcal{F}}_R H \mathcal{E}_L + h.c., \quad (\text{A.7})$$

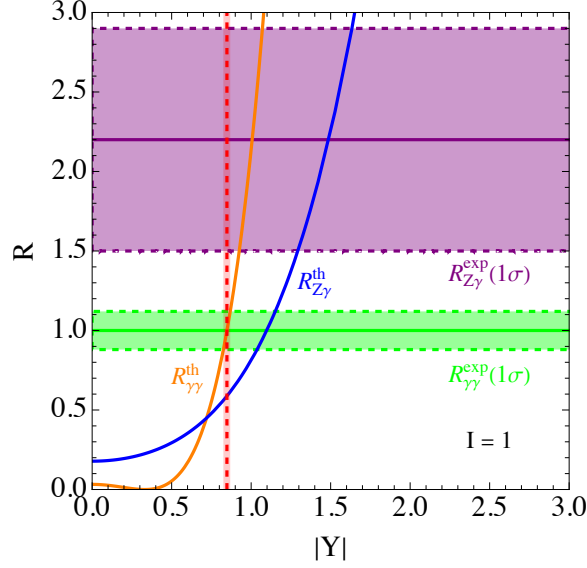


Figure 8: $R_{\gamma\gamma}$ and $R_{Z\gamma}$ signal strengths as a function of $|Y|$ for $I = 1$. The area between the shaded lines around the central value corresponds to the current 1σ experimental uncertainty. The red, vertical band denotes the values of Y able to satisfy the di-photon constraints at 1σ .

where isospin contractions are left implicit. The Lagrangian in Eq. (A.7) admits two global symmetries, which are

$$U(1)_V : \mathcal{L} \rightarrow e^{i\alpha} \mathcal{L}, \quad \mathcal{E} \rightarrow e^{i\alpha} \mathcal{E}, \quad \mathcal{N} \rightarrow e^{i\alpha} \mathcal{N}, \quad \mathcal{F} \rightarrow e^{i\alpha} \mathcal{F}, \quad (\text{A.8})$$

$$U(1)_A : \mathcal{L} \rightarrow e^{i\beta\gamma_5} \mathcal{L}, \quad \mathcal{E} \rightarrow e^{-i\beta\gamma_5} \mathcal{E}, \quad \mathcal{N} \rightarrow e^{-i\beta\gamma_5} \mathcal{N}, \quad \mathcal{F} \rightarrow e^{i\beta\gamma_5} \mathcal{F}, \quad (\text{A.9})$$

that can prevent any additional Yukawa or mass term that involves the exotic fields. Let us consider the case in which no other mass term or mass mixing with the SM fields is present. Assuming the exotic fermions to be much heavier than the Higgs and Z bosons after EWSB, one gets the following BSM contribution to $h \rightarrow \gamma\gamma, Z\gamma$ decays

$$A_{\gamma\gamma}^{\text{BSM}} \simeq \frac{16}{9} I(1 + 2I^2 + 6Y^2), \quad (\text{A.10})$$

$$A_{Z\gamma}^{\text{BSM}} \simeq \frac{4}{9} I(1 + \text{tg}_w^2)(1 + 8I^2) - \frac{16}{9} I(1 + 2I^2 + 6Y^2) \text{tg}_w^2. \quad (\text{A.11})$$

For $I \geq 3/2$ the di-photon theoretical prediction is above the experimental result for all the values of Y so we are left with only two relevant cases, which are $I = 1/2$, already investigated in the main text, and $I = 1$. We plot the 1σ experimental regions and theoretical predictions of $R_{\gamma\gamma, Z\gamma}$ for $I = 1$ in Fig. 8. Note that for $I = 1$, one gets $Y = 0.848_{-0.023}^{+0.021}$ from the requirement of matching the $R_{\gamma\gamma}$ result at 1σ , thus leading to the prediction $R_{Z\gamma} = 0.588_{-0.028}^{+0.026}$, which is smaller than the SM value and in contrast with the recent experimental observation.

B General formulae for loop-induced Higgs couplings and oblique corrections

In this Appendix we present the calculation of the effective loop-induced Higgs couplings to gauge bosons that arise after integrating out heavy fermionic degrees of freedom and the contribution of the latter to the Peskin-Takeuchi parameters S and T . In particular, we focus on the 3-point vertices hVV' when gauge invariance prevents renormalizable couplings to the Higgs field, such that the tree level amplitudes are zero and one-loop amplitudes are free from UV divergences.

B.1 General setup

We assume a general setup with a set of gauge bosons G_μ^A related to the generators Q^A of the gauge symmetry group \mathcal{G} , that can be in general semi-simple. The model contains a fermionic sector, whose fields are labeled as ψ_i , that acquire a mass term \mathcal{M}_{ij} after a spontaneous symmetry breaking mechanism. The $(\frac{1}{2}, 0)$ and $(0, \frac{1}{2})$ Lorentz components of the ψ field are separately reducible representations of \mathcal{G} and the generators act on them as

$$Q^A \psi_i = \sum_j (Q_L^A)_{ij} \psi_{jL} + \sum_j (Q_R^A)_{ij} \psi_{jR}, \quad (\text{B.1})$$

where $(Q_{L,R}^A)_{ij}$ are the matrix representation of the gauge multiplets $\psi_{L,R} \equiv P_{L,R} \psi$. We restrict ourselves to models with a $U(1)_\psi$ symmetry corresponding to the fermionic number of the ψ fields, $\psi_i \rightarrow e^{i\phi} \psi_i$. The real scalar Higgs fields, responsible for the spontaneous symmetry breaking mechanism, are labeled as $H_a = (H_a)^*$ and belong to a reducible representation of the gauge group \mathcal{G} . By performing an infinitesimal transformation of angle α_A along the Q^A generator, the H_a fields transform like

$$\delta H_a = \sum_b g_A \alpha_A (iQ_H^A)_{ab} H_b, \quad (\text{B.2})$$

where $(iQ_H^A)_{ab}$ is a real and antisymmetric matrix. Hence,

$$\mathcal{L} \supset \sum_i \bar{\psi}_i i \not{\partial} \psi_i - \sum_{a,i,j} H_a (\bar{\psi}_{iL} \mathcal{Y}_{ij}^a \psi_{jR} + \text{h.c.}) - \sum_A g_A G_\mu^A J^{\mu A}, \quad (\text{B.3})$$

with

$$J^{\mu A} = \sum_{i,j} \left[\bar{\psi}_{iL} \gamma^\mu (Q_L^A)_{ij} \psi_{jL} + \bar{\psi}_{iR} \gamma^\mu (Q_R^A)_{ij} \psi_{jR} \right]. \quad (\text{B.4})$$

The Yukawa couplings must preserve gauge invariance and hence they satisfy

$$\sum_k \mathcal{Y}_{ik}^a (Q_R^A)_{kj} - \sum_k (Q_L^A)_{ik} \mathcal{Y}_{kj}^a + \sum_b \mathcal{Y}_{ij}^b (Q_H^A)_{ba} = 0. \quad (\text{B.5})$$

The Higgs fields acquire the VEVs $\langle H_a \rangle = v_a$ which break the gauge group, leaving an unbroken subgroup \mathcal{G}_0 . Then, the mass matrix of the ψ fields is given by

$$\mathcal{M}_{ij} = \sum_a \mathcal{Y}_{ij}^a v_a, \quad (\text{B.6})$$

leading to

$$\begin{aligned} \mathcal{L} \supset & \sum_i \bar{\psi}_i i \not{\partial} \psi_i - \sum_{i,j} (\bar{\psi}_{iL} \mathcal{M}_{ij} \psi_{jR} + \text{h.c.}) \\ & - \sum_{a,i,j} \tilde{H}_a (\bar{\psi}_{iL} \mathcal{Y}_{ij}^a \psi_{jR} + \text{h.c.}) - \sum_A g_A G_\mu^A J^{\mu A}, \end{aligned} \quad (\text{B.7})$$

where $\tilde{H}_a = H_a - v_a$ are the Higgs fluctuations around the vacuum.

In order to go in the mass basis, the mass matrix \mathcal{M} is diagonalized via the bi-unitary transformations $\psi_R \rightarrow U_R \psi_R$ and $\psi_L \rightarrow U_L \psi_L$, which by construction satisfy $U_L^\dagger \mathcal{M} U_R = \text{diag}(m_1, m_2, \dots)$. This yields

$$\mathcal{L} \supset \sum_i \bar{\psi}_i (i \not{\partial} - m_i) \psi_i - \sum_A g_A G_\mu^A J_U^{\mu A} - \sum_{a,i,j} \tilde{H}_a \bar{\psi}_i (\hat{\mathcal{Y}}_R^a P_R + \hat{\mathcal{Y}}_L^a P_L)_{ij} \psi_j, \quad (\text{B.8})$$

where $\hat{\mathcal{Y}}_R^a = U_L^\dagger \mathcal{Y}^a U_R = (\hat{\mathcal{Y}}_L^a)^\dagger$, while the gauge currents in the mass basis are equal to

$$J_U^{\mu A} = \sum_{i,j} \left[\bar{\psi}_{iL} \gamma^\mu (U_L^\dagger Q_L^A U_L)_{ij} \psi_{jL} + \bar{\psi}_{iR} \gamma^\mu (U_R^\dagger Q_R^A U_R)_{ij} \psi_{jR} \right]. \quad (\text{B.9})$$

B.2 Loop-induced Higgs couplings

After integrating out the heavy fermion fields, we get effective operators of the type⁶

$$\begin{aligned} \mathcal{L} \supset & \sum_{a,B,C} C_{aBC} \tilde{H}_a (\partial_\alpha G_\mu^B - \partial_\mu G_\alpha^B) (\partial_\alpha G_\mu^C - \partial_\mu G_\alpha^C) \\ & - \sum_{a,B,C} D_{aBC} \epsilon^{\mu\nu\alpha\beta} \tilde{H}_a (\partial_\alpha G_\mu^B - \partial_\mu G_\alpha^B) (\partial_\beta G_\nu^C - \partial_\nu G_\beta^C), \end{aligned} \quad (\text{B.10})$$

in terms of the effective field theory coefficients $C_{aBC} = C_{aCB}$ and $D_{aBC} = D_{aCB}$ that we want to compute.

B.2.1 1-loop matching

Loop-induced Higgs coupling occurs in the 3-point functions $\Gamma_{ABC}^{\alpha\mu\nu}(x, y, z)$ and $\Gamma_{aBC}^{\mu\nu}(x, y, z)$ at 1-loop through fermionic triangle diagrams, see Fig. 9. The amplitudes in momentum space are defined via

$$\int d^4x d^4y d^4z e^{i(xq_1 + yq_2 + zq_3)} \Gamma_{aBC}^{\mu\nu}(x, y, z)|_{1\text{-loop}} = (2\pi)^4 \delta^{(4)}(q_1 + q_2 + q_3) \mu^{\frac{4-d}{2}} iM_{aBC}^{\mu\nu}(q_1, q_2, q_3). \quad (\text{B.11})$$

which yield

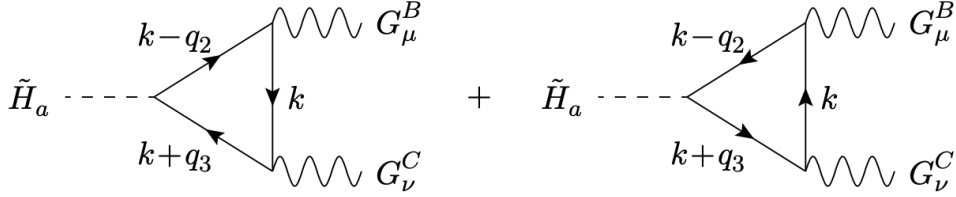


Figure 9: Feynman diagrams relative to the 3-point functions in Eq. (B.11).

$$\begin{aligned} M_{aBC}^{\mu\nu} = & \sum_{\substack{i,j,k \\ \chi_1, \chi_2, \chi_3}} g_B g_C (\hat{\mathcal{Y}}_{\chi_1}^a)_{jk} (U_{\chi_2}^\dagger Q_{\chi_2}^B U_{\chi_2})_{ki} (U_{\chi_3}^\dagger Q_{\chi_3}^C U_{\chi_3})_{ij} \\ & \times i\mu^{4-d} \int \frac{d^d k}{(2\pi)^d} \frac{\text{Tr}_D[\gamma^\mu P_{\chi_2}(\not{k} + m_i) \gamma^\nu P_{\chi_3}(\not{k} + \not{q}_3 + m_j) P_{\chi_1}(\not{k} - \not{q}_2 + m_k)]}{[k^2 - m_i^2][(k + q_3)^2 - m_j^2][(k - q_2)^2 - m_k^2]} \\ & + \sum_{\substack{i,j,k \\ \chi_1, \chi_2, \chi_3}} g_B g_C (\hat{\mathcal{Y}}_{\chi_1}^a)_{kj} (U_{\chi_3}^\dagger Q_{\chi_3}^C U_{\chi_3})_{ji} (U_{\chi_2}^\dagger Q_{\chi_2}^B U_{\chi_2})_{ik} \\ & \times i\mu^{4-d} \int \frac{d^d k}{(2\pi)^d} \frac{\text{Tr}_D[\gamma^\nu P_{\chi_3}(\not{k} + m_i) \gamma^\mu P_{\chi_2}(\not{k} + \not{q}_2 + m_k) P_{\chi_1}(\not{k} - \not{q}_3 + m_j)]}{[k^2 - m_i^2][(k + q_2)^2 - m_k^2][(k - q_3)^2 - m_j^2]}, \end{aligned} \quad (\text{B.12})$$

where we have regularized the theory with dimensional regularization. One finds that the $q_3^\mu q_2^\nu$ and $\epsilon^{\mu\nu\alpha\beta}$ terms we are interested in are finite, *i.e.* they do not contain $1/(d-4)$ poles, and are independent from the renormalization scale μ ⁷. Hence, we are free to send $d \rightarrow 4$. In order to obtain the effective field theory coefficients in Eq. (B.10), we have to match the expressions

⁶We fix $\epsilon^{0123} = 1$.

⁷Instead, the term proportional to $g^{\mu\nu}$ could be affected by a divergence if the vertex is allowed at tree level but we assume the presence of a unbroken gauge symmetry that forbid the tree-level vertex and hence resolve the divergence. So we only focus on the finite terms of the 1-loop amplitude.

that we have calculated above to the effective field theory matrix elements in the limit of heavy fermion masses, i.e.

$$\lim_{\substack{m_{i,j,k}^2 \gg \\ q_2^2, q_3^2, q_2 q_3}} M_{aBC}^{\mu\nu} = 4C_{aBC}[q_3^\mu q_2^\nu - (q_3 \cdot q_2)g^{\mu\nu}] + 8D_{aBC}\epsilon^{\mu\nu\alpha\beta} q_{2\alpha} q_{3\beta}. \quad (\text{B.13})$$

Finally we get

$$\begin{aligned} C_{aBC} = & \frac{g_B g_C}{32\pi^2} \int_0^{+\infty} ds \int_0^1 dx \int_0^1 dy \int_0^1 dz 2\delta(1-x-y-z) \times \\ & \times \text{Re} \left\{ x \text{Tr} \left[\mathcal{Y}^a e^{-sz\mathcal{M}^\dagger \mathcal{M}} Q_R^B e^{-sx\mathcal{M}^\dagger \mathcal{M}} \mathcal{M}^\dagger Q_L^C e^{-sy\mathcal{M}\mathcal{M}^\dagger} \right] \right. \\ & + x \text{Tr} \left[\mathcal{Y}^a e^{-sz\mathcal{M}^\dagger \mathcal{M}} Q_R^C e^{-sx\mathcal{M}^\dagger \mathcal{M}} \mathcal{M}^\dagger Q_L^B e^{-sy\mathcal{M}\mathcal{M}^\dagger} \right] \\ & + y(1-2z) \text{Tr} \left[\mathcal{Y}^a e^{-sz\mathcal{M}^\dagger \mathcal{M}} Q_R^B e^{-sx\mathcal{M}^\dagger \mathcal{M}} Q_R^C \mathcal{M}^\dagger e^{-sy\mathcal{M}\mathcal{M}^\dagger} \right] \\ & + y(1-2z) \text{Tr} \left[\mathcal{Y}^a e^{-sz\mathcal{M}^\dagger \mathcal{M}} Q_R^C e^{-sx\mathcal{M}^\dagger \mathcal{M}} Q_R^B \mathcal{M}^\dagger e^{-sy\mathcal{M}\mathcal{M}^\dagger} \right] \\ & + z(1-2y) \text{Tr} \left[\mathcal{Y}^a e^{-sz\mathcal{M}^\dagger \mathcal{M}} \mathcal{M}^\dagger Q_L^B e^{-sx\mathcal{M}\mathcal{M}^\dagger} Q_L^C e^{-sy\mathcal{M}\mathcal{M}^\dagger} \right] \\ & \left. + z(1-2y) \text{Tr} \left[\mathcal{Y}^a e^{-sz\mathcal{M}^\dagger \mathcal{M}} \mathcal{M}^\dagger Q_L^C e^{-sx\mathcal{M}\mathcal{M}^\dagger} Q_L^B e^{-sy\mathcal{M}\mathcal{M}^\dagger} \right] \right\}, \end{aligned} \quad (\text{B.14})$$

and

$$\begin{aligned} D_{aBC} = & \frac{g_B g_C}{64\pi^2} \int_0^{+\infty} ds \int_0^1 dx \int_0^1 dy \int_0^1 dz 2\delta(1-x-y-z) \times \\ & \times \text{Im} \left\{ x \text{Tr} \left[e^{-sz\mathcal{M}^\dagger \mathcal{M}} Q_R^B \mathcal{M}^\dagger e^{-sx\mathcal{M}\mathcal{M}^\dagger} Q_L^C e^{-sy\mathcal{M}\mathcal{M}^\dagger} \mathcal{Y}^a \right] \right. \\ & + x \text{Tr} \left[e^{-sz\mathcal{M}^\dagger \mathcal{M}} Q_R^C \mathcal{M}^\dagger e^{-sx\mathcal{M}\mathcal{M}^\dagger} Q_L^B e^{-sy\mathcal{M}\mathcal{M}^\dagger} \mathcal{Y}^a \right] \\ & + y \text{Tr} \left[e^{-sz\mathcal{M}^\dagger \mathcal{M}} Q_R^B e^{-sx\mathcal{M}^\dagger \mathcal{M}} Q_R^C \mathcal{M}^\dagger e^{-sy\mathcal{M}\mathcal{M}^\dagger} \mathcal{Y}^a \right] \\ & + y \text{Tr} \left[e^{-sz\mathcal{M}^\dagger \mathcal{M}} Q_R^C e^{-sx\mathcal{M}^\dagger \mathcal{M}} Q_R^B \mathcal{M}^\dagger e^{-sy\mathcal{M}\mathcal{M}^\dagger} \mathcal{Y}^a \right] \\ & + z \text{Tr} \left[e^{-sz\mathcal{M}^\dagger \mathcal{M}} \mathcal{M}^\dagger Q_L^C e^{-sx\mathcal{M}\mathcal{M}^\dagger} Q_L^B e^{-sy\mathcal{M}\mathcal{M}^\dagger} \mathcal{Y}^a \right] \\ & \left. + z \text{Tr} \left[e^{-sz\mathcal{M}^\dagger \mathcal{M}} \mathcal{M}^\dagger Q_L^B e^{-sx\mathcal{M}\mathcal{M}^\dagger} Q_L^C e^{-sy\mathcal{M}\mathcal{M}^\dagger} \mathcal{Y}^a \right] \right\}. \end{aligned} \quad (\text{B.15})$$

B.2.2 Application to $h \rightarrow \gamma\gamma, Z\gamma$

Our results can be applied to the case of $h \rightarrow \gamma\gamma, Z\gamma$ if $B = \gamma$ and $C = Z$, for which

$$g_\gamma = e, \quad g_Z = \frac{g}{c_w}, \quad Q^\gamma = Q \quad \text{and} \quad Q^Z = T^3 - s_w^2 Q, \quad (\text{B.16})$$

where T^3 is the diagonal isospin and Q is the electric charge. By defining

$$R_{\gamma\gamma, Z\gamma} = \frac{|A_{\gamma\gamma, Z\gamma}^{\text{SM}} + A_{\gamma\gamma, Z\gamma}^{\text{BSM}}|^2 + |\tilde{A}_{\gamma\gamma, Z\gamma}^{\text{BSM}}|^2}{|A_{\gamma\gamma, Z\gamma}^{\text{SM}}|^2}, \quad (\text{B.17})$$

with $A_{\gamma\gamma}^{\text{SM}} \simeq -6.5$, $A_{Z\gamma}^{\text{SM}} \simeq -6.64$, one gets

$$A_{\gamma\gamma}^{\text{BSM}} \simeq \frac{2}{3}v \operatorname{Re} \left\{ \operatorname{Tr} \left[Q_R^2 \mathcal{M}^{-1} \mathcal{Y}^h \right] + \operatorname{Tr} \left[Q_L^2 \mathcal{Y}^h \mathcal{M}^{-1} \right] \right\}, \quad (\text{B.18})$$

$$\tilde{A}_{\gamma\gamma}^{\text{BSM}} \simeq v \operatorname{Im} \left\{ \operatorname{Tr} \left[Q_R^2 \mathcal{M}^{-1} \mathcal{Y}^h \right] + \operatorname{Tr} \left[Q_L^2 \mathcal{Y}^h \mathcal{M}^{-1} \right] \right\}, \quad (\text{B.19})$$

$$A_{Z\gamma}^{\text{BSM}} \simeq \frac{v}{c_w} \int_0^{+\infty} ds \int_0^1 dz 2z^2 \times \operatorname{Re} \left\{ \operatorname{Tr} \left[Q_R (T_R^3 - s_w^2 Q_R) e^{-sz \mathcal{M}^\dagger \mathcal{M}} \mathcal{M}^\dagger \mathcal{Y}^h e^{-s(1-z) \mathcal{M}^\dagger \mathcal{M}} \right] + \operatorname{Tr} \left[Q_L (T_L^3 - s_w^2 Q_L) e^{-s(1-z) \mathcal{M} \mathcal{M}^\dagger} \mathcal{Y}^h \mathcal{M}^\dagger e^{-sz \mathcal{M} \mathcal{M}^\dagger} \right] \right\}, \quad (\text{B.20})$$

$$\tilde{A}_{Z\gamma}^{\text{BSM}} \simeq \frac{v}{c_w} \int_0^{+\infty} ds \int_0^1 dz 2z \times \operatorname{Im} \left\{ \operatorname{Tr} \left[Q_R (T_R^3 - s_w^2 Q_R) e^{-sz \mathcal{M}^\dagger \mathcal{M}} \mathcal{M}^\dagger \mathcal{Y}^h e^{-s(1-z) \mathcal{M}^\dagger \mathcal{M}} \right] + \operatorname{Tr} \left[Q_L (T_L^3 - s_w^2 Q_L) e^{-s(1-z) \mathcal{M} \mathcal{M}^\dagger} \mathcal{Y}^h \mathcal{M}^\dagger e^{-sz \mathcal{M} \mathcal{M}^\dagger} \right] \right\}. \quad (\text{B.21})$$

Here we simplified the expressions above making use of the relation

$$\mathcal{M} Q_R - Q_L \mathcal{M} = \mathcal{Y}^h Q_R - Q_L \mathcal{Y}^h = 0, \quad (\text{B.22})$$

due to the fact that the electric charge correspond to an unbroken gauge symmetry and the Higgs field h is uncharged under it. Note that if the h field couples to the fermions through the substitution $v \rightarrow v + h$, the Yukawa coupling matrix of the Higgs can be written as

$$\mathcal{Y}^h = \frac{\partial}{\partial v} \mathcal{M}. \quad (\text{B.23})$$

B.3 Oblique corrections

The gauge boson propagators get radiative correction from loops. Fermion contributions to the vacuum polarization functions come from 1-loop such as shown in Fig. 10. After integrating out the heavy fermion fields, one gets

$$\begin{aligned} \Pi_{BC}^{\mu\nu} &= \sum_{\substack{i,j \\ \chi_1, \chi_2}} g_B g_C (U_{\chi_2}^\dagger Q_{\chi_2}^B U_{\chi_2})_{ji} (U_{\chi_3}^\dagger Q_{\chi_3}^C U_{\chi_3})_{ij} \\ &\times i\mu^{4-d} \int \frac{d^d k}{(2\pi)^d} \frac{\operatorname{Tr}_D [\gamma^\mu P_{\chi_1} (\not{k} + m_i) \gamma^\nu P_{\chi_2} (\not{k} + \not{q} + m_j)]}{[k^2 - m_i^2] [(k+q)^2 - m_j^2]} \\ &= \Pi_{BC}(q^2) g^{\mu\nu} + q^\mu q^\nu \text{-terms}, \end{aligned} \quad (\text{B.24})$$

where we introduced dimensional regularization. Expanding with $d = 4 - \epsilon$, one gets

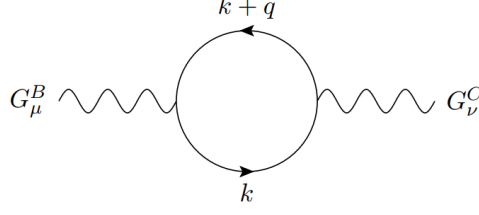


Figure 10: Feynman diagram relative to the vacuum polarization functions in Eq. (B.24).

$$\begin{aligned}
\Pi_{BC}(q^2) = \Pi_{CB}(q^2) = & \frac{g_B g_C}{4\pi^2} \frac{1}{\epsilon} \left\{ \frac{1}{2} \text{Tr} \left[Q_R^B \mathcal{M}^\dagger \mathcal{M} Q_R^C + Q_R^B Q_R^C \mathcal{M}^\dagger \mathcal{M} \right] \right. \\
& + \frac{1}{2} \text{Tr} \left[Q_L^B \mathcal{M} \mathcal{M}^\dagger Q_L^C + Q_L^B Q_L^C \mathcal{M} \mathcal{M}^\dagger \right] \\
& - \text{Tr} \left[Q_R^B \mathcal{M}^\dagger Q_L^C \mathcal{M} + Q_L^B \mathcal{M} Q_R^C \mathcal{M}^\dagger \right] \\
& \left. - \frac{q^2}{3} \text{Tr} \left[Q_R^B Q_R^C + Q_L^B Q_L^C \right] \right\} \\
- \frac{g_B g_C}{8\pi^2} \int_0^1 dz \int_0^{+\infty} ds \frac{1}{s} \left\{ & 2z(1-z)q^2 e^{sz(1-z)q^2} \text{Tr} \left[Q_R^B e^{-s(1-z)\mathcal{M}^\dagger \mathcal{M}} Q_R^C e^{-sz\mathcal{M}^\dagger \mathcal{M}} \right] \right. \\
& + 2z(1-z)q^2 e^{sz(1-z)q^2} \text{Tr} \left[Q_L^B e^{-s(1-z)\mathcal{M} \mathcal{M}^\dagger} Q_L^C e^{-sz\mathcal{M} \mathcal{M}^\dagger} \right] \\
& - 2z(1-z)q^2 e^{-s\tilde{\mu}^2} \text{Tr} \left[Q_R^B Q_R^C + Q_L^B Q_L^C \right] \\
& - ze^{sz(1-z)q^2} \text{Tr} \left[Q_R^B e^{-s(1-z)\mathcal{M}^\dagger \mathcal{M}} Q_R^C \mathcal{M}^\dagger \mathcal{M} e^{-sz\mathcal{M}^\dagger \mathcal{M}} \right] \\
& - ze^{sz(1-z)q^2} \text{Tr} \left[Q_L^B e^{-s(1-z)\mathcal{M} \mathcal{M}^\dagger} Q_L^C \mathcal{M} \mathcal{M}^\dagger e^{-sz\mathcal{M} \mathcal{M}^\dagger} \right] \\
& + ze^{-s\tilde{\mu}^2} \text{Tr} \left[Q_R^B Q_R^C \mathcal{M}^\dagger \mathcal{M} + Q_L^B Q_L^C \mathcal{M} \mathcal{M}^\dagger \right] \\
& - (1-z)e^{sz(1-z)q^2} \text{Tr} \left[Q_R^B \mathcal{M}^\dagger \mathcal{M} e^{-s(1-z)\mathcal{M}^\dagger \mathcal{M}} Q_R^C e^{-sz\mathcal{M}^\dagger \mathcal{M}} \right] \\
& - (1-z)e^{sz(1-z)q^2} \text{Tr} \left[Q_L^B \mathcal{M} \mathcal{M}^\dagger e^{-s(1-z)\mathcal{M} \mathcal{M}^\dagger} Q_L^C e^{-sz\mathcal{M} \mathcal{M}^\dagger} \right] \\
& + (1-z)e^{-s\tilde{\mu}^2} \text{Tr} \left[Q_R^B \mathcal{M}^\dagger \mathcal{M} Q_R^C + Q_L^B \mathcal{M} \mathcal{M}^\dagger Q_L^C \right] \\
& + e^{sz(1-z)q^2} \text{Tr} \left[Q_R^B e^{-s(1-z)\mathcal{M}^\dagger \mathcal{M}} \mathcal{M}^\dagger Q_L^C \mathcal{M} e^{-sz\mathcal{M}^\dagger \mathcal{M}} \right] \\
& + e^{sz(1-z)q^2} \text{Tr} \left[Q_L^B e^{-s(1-z)\mathcal{M} \mathcal{M}^\dagger} \mathcal{M} Q_R^C \mathcal{M}^\dagger e^{-sz\mathcal{M} \mathcal{M}^\dagger} \right] \\
& \left. - e^{-s\tilde{\mu}^2} \text{Tr} \left[Q_R^B \mathcal{M}^\dagger Q_L^C \mathcal{M} + Q_L^B \mathcal{M} Q_R^C \mathcal{M}^\dagger \right] \right\}, \tag{B.25}
\end{aligned}$$

where $\tilde{\mu} = 4\pi e^{-\gamma_E} \mu$, with γ_E being the Euler–Mascheroni constant.

B.3.1 Peskin-Takeuchi parameters

The Peskin-Takeuchi parameters S and T are defined through the vacuum polarization functions $\Pi(q^2)$ as

$$T \equiv \frac{1}{\alpha} \left(\frac{\Pi_{WW}^{\text{BSM}}(0)}{m_W^2} - \frac{\Pi_{ZZ}^{\text{BSM}}(0)}{m_Z^2} \right), \quad (\text{B.26})$$

$$S \equiv \frac{4s_w^2 c_w^2}{\alpha} \left[\frac{\Pi_{ZZ}^{\text{BSM}}(m_Z^2) - \Pi_{ZZ}^{\text{BSM}}(0)}{m_Z^2} - \frac{c_w^2 - s_w^2}{c_w s_w} \frac{\Pi_{Z\gamma}^{\text{BSM}}(m_Z^2)}{m_Z^2} - \frac{\Pi_{\gamma\gamma}^{\text{BSM}}(m_Z^2)}{m_Z^2} \right] \\ \simeq \frac{4s_w^2 c_w^2}{\alpha} \left[\Pi'_{ZZ, \text{BSM}}(0) - \frac{c_w^2 - s_w^2}{c_w s_w} \Pi'_{Z\gamma, \text{BSM}}(0) - \Pi'_{\gamma\gamma, \text{BSM}}(0) \right], \quad (\text{B.27})$$

where the last approximation holds if the new physics is much heavier than the SM bosons. We then obtain

$$T = \frac{1}{4\pi s_w^2 c_w^2 m_Z^2} \int_0^1 dz \int_0^{+\infty} ds \frac{1}{s} \left\{ (1-z) \text{Tr} \left[T_R^+ e^{-sz\mathcal{M}^\dagger \mathcal{M}} T_R^- e^{-s(1-z)\mathcal{M}^\dagger \mathcal{M}} \mathcal{M}^\dagger \mathcal{M} \right] \right. \\ + (1-z) \text{Tr} \left[T_R^- e^{-sz\mathcal{M}^\dagger \mathcal{M}} T_R^+ e^{-s(1-z)\mathcal{M}^\dagger \mathcal{M}} \mathcal{M}^\dagger \mathcal{M} \right] \\ - 4(1-z) \text{Tr} \left[T_R^3 e^{-sz\mathcal{M}^\dagger \mathcal{M}} T_R^3 e^{-s(1-z)\mathcal{M}^\dagger \mathcal{M}} \mathcal{M}^\dagger \mathcal{M} \right] \\ + (1-z) \text{Tr} \left[T_L^+ e^{-sz\mathcal{M}\mathcal{M}^\dagger} T_L^- e^{-s(1-z)\mathcal{M}\mathcal{M}^\dagger} \mathcal{M}\mathcal{M}^\dagger \right] \\ + (1-z) \text{Tr} \left[T_L^- e^{-sz\mathcal{M}\mathcal{M}^\dagger} T_L^+ e^{-s(1-z)\mathcal{M}\mathcal{M}^\dagger} \mathcal{M}\mathcal{M}^\dagger \right] \\ - 4(1-z) \text{Tr} \left[T_L^3 e^{-sz\mathcal{M}\mathcal{M}^\dagger} T_L^3 e^{-s(1-z)\mathcal{M}\mathcal{M}^\dagger} \mathcal{M}\mathcal{M}^\dagger \right] \\ + \text{Tr} \left[T_R^+ e^{-sz\mathcal{M}^\dagger \mathcal{M}} \mathcal{M}^\dagger T_L^- e^{-s(1-z)\mathcal{M}\mathcal{M}^\dagger} \mathcal{M} \right] \\ + \text{Tr} \left[T_R^- e^{-sz\mathcal{M}^\dagger \mathcal{M}} \mathcal{M}^\dagger T_L^+ e^{-s(1-z)\mathcal{M}\mathcal{M}^\dagger} \mathcal{M} \right] \\ \left. - 4 \text{Tr} \left[T_R^3 e^{-sz\mathcal{M}^\dagger \mathcal{M}} \mathcal{M}^\dagger T_L^3 e^{-s(1-z)\mathcal{M}\mathcal{M}^\dagger} \mathcal{M} \right] \right\}, \quad (\text{B.28})$$

where $T^\pm = (T^1 \pm iT^2)/\sqrt{2}$ are the non-diagonal isospin generators, and

$$\begin{aligned}
S \simeq \frac{2}{\pi} \int_0^1 dz z(1-z) \int_0^{+\infty} ds \left\{ \text{Tr} \left[T_R^3 e^{-sz\mathcal{M}^\dagger\mathcal{M}} \mathcal{M}^\dagger T_L^Y \mathcal{M} e^{-s(1-z)\mathcal{M}^\dagger\mathcal{M}} \right] \right. \\
+ \text{Tr} \left[T_L^3 e^{-sz\mathcal{M}\mathcal{M}^\dagger} \mathcal{M} T_R^Y \mathcal{M}^\dagger e^{-s(1-z)\mathcal{M}\mathcal{M}^\dagger} \right] \\
- (1-z) \text{Tr} \left[T_R^3 e^{-sz\mathcal{M}^\dagger\mathcal{M}} T_R^Y e^{-s(1-z)\mathcal{M}^\dagger\mathcal{M}} \mathcal{M}^\dagger \mathcal{M} \right] \\
- (1-z) \text{Tr} \left[T_R^Y e^{-sz\mathcal{M}^\dagger\mathcal{M}} T_R^3 e^{-s(1-z)\mathcal{M}^\dagger\mathcal{M}} \mathcal{M}^\dagger \mathcal{M} \right] \\
- (1-z) \text{Tr} \left[T_L^3 e^{-sz\mathcal{M}\mathcal{M}^\dagger} T_L^Y e^{-s(1-z)\mathcal{M}\mathcal{M}^\dagger} \mathcal{M}\mathcal{M}^\dagger \right] \\
- (1-z) \text{Tr} \left[T_L^Y e^{-sz\mathcal{M}\mathcal{M}^\dagger} T_L^3 e^{-s(1-z)\mathcal{M}\mathcal{M}^\dagger} \mathcal{M}\mathcal{M}^\dagger \right] \\
+ \frac{1}{s} \text{Tr} \left[T_R^3 e^{-sz\mathcal{M}^\dagger\mathcal{M}} T_R^Y e^{-s(1-z)\mathcal{M}^\dagger\mathcal{M}} \right] \\
+ \left. \frac{1}{s} \text{Tr} \left[T_L^3 e^{-sz\mathcal{M}\mathcal{M}^\dagger} T_L^Y e^{-s(1-z)\mathcal{M}\mathcal{M}^\dagger} \right] \right\}, \tag{B.29}
\end{aligned}$$

where T^Y is the hypercharge generator.

References

- [1] B. Holdom, W. S. Hou, T. Hurth, M. L. Mangano, S. Sultansoy, and G. Unel, ‘‘Four Statements about the Fourth Generation,’’ *PMC Phys. A* **3** (2009) 4, [arXiv:0904.4698 \[hep-ph\]](#).
- [2] G. D. Kribs, T. Plehn, M. Spannowsky, and T. M. P. Tait, ‘‘Four generations and Higgs physics,’’ *Phys. Rev. D* **76** (2007) 075016, [arXiv:0706.3718 \[hep-ph\]](#).
- [3] E. Kuflik, Y. Nir, and T. Volansky, ‘‘Implications of Higgs searches on the four generation standard model,’’ *Phys. Rev. Lett.* **110** no. 9, (2013) 091801, [arXiv:1204.1975 \[hep-ph\]](#).
- [4] O. Eberhardt, G. Herbert, H. Lacker, A. Lenz, A. Menzel, U. Nierste, and M. Wiebusch, ‘‘Impact of a Higgs boson at a mass of 126 GeV on the standard model with three and four fermion generations,’’ *Phys. Rev. Lett.* **109** (2012) 241802, [arXiv:1209.1101 \[hep-ph\]](#).
- [5] N. Bizot and M. Frigerio, ‘‘Fermionic extensions of the Standard Model in light of the Higgs couplings,’’ *JHEP* **01** (2016) 036, [arXiv:1508.01645 \[hep-ph\]](#).
- [6] Q. Bonnefoy, L. Di Luzio, C. Grojean, A. Paul, and A. N. Rossia, ‘‘The anomalous case of axion EFTs and massive chiral gauge fields,’’ *JHEP* **07** (2021) 189, [arXiv:2011.10025 \[hep-ph\]](#).
- [7] M. Duerr, P. Fileviez Perez, and M. B. Wise, ‘‘Gauge Theory for Baryon and Lepton Numbers with Leptoquarks,’’ *Phys. Rev. Lett.* **110** (2013) 231801, [arXiv:1304.0576 \[hep-ph\]](#).
- [8] M. Duerr and P. Fileviez Perez, ‘‘Baryonic Dark Matter,’’ *Phys. Lett. B* **732** (2014) 101–104, [arXiv:1309.3970 \[hep-ph\]](#).
- [9] B. A. Dobrescu and C. Frugiuele, ‘‘Hidden GeV-scale interactions of quarks,’’ *Phys. Rev. Lett.* **113** (2014) 061801, [arXiv:1404.3947 \[hep-ph\]](#).
- [10] B. A. Dobrescu, ‘‘Leptophobic Boson Signals with Leptons, Jets and Missing Energy,’’ [arXiv:1506.04435 \[hep-ph\]](#).
- [11] J. A. Dror, R. Lasenby, and M. Pospelov, ‘‘New constraints on light vectors coupled to anomalous currents,’’ *Phys. Rev. Lett.* **119** no. 14, (2017) 141803, [arXiv:1705.06726 \[hep-ph\]](#).

- [12] J. A. Dror, R. Lasenby, and M. Pospelov, “Dark forces coupled to nonconserved currents,” *Phys. Rev. D* **96** no. 7, (2017) 075036, [arXiv:1707.01503 \[hep-ph\]](#).
- [13] L. Di Luzio, M. Nardecchia, and C. Toni, “Light vectors coupled to anomalous currents with harmless Wess-Zumino terms,” *Phys. Rev. D* **105** no. 11, (2022) 115042, [arXiv:2204.05945 \[hep-ph\]](#).
- [14] **CMS, ATLAS** Collaboration, G. Aad *et al.*, “Evidence for the Higgs boson decay to a Z boson and a photon at the LHC,” [arXiv:2309.03501 \[hep-ex\]](#).
- [15] S. Banerjee, M. Frank, and S. K. Rai, “Higgs data confronts Sequential Fourth Generation Fermions in the Higgs Triplet Model,” *Phys. Rev. D* **89** no. 7, (2014) 075005, [arXiv:1312.4249 \[hep-ph\]](#).
- [16] B. Holdom, “The accidental Higgs boson,” *Phys. Rev. D* **90** no. 1, (2014) 015004, [arXiv:1404.6229 \[hep-ph\]](#).
- [17] D. Das, A. Kundu, and I. Saha, “Higgs data does not rule out a sequential fourth generation with an extended scalar sector,” *Phys. Rev. D* **97** no. 1, (2018) 011701, [arXiv:1707.03000 \[hep-ph\]](#).
- [18] R. T. D’Agnolo, F. Nortier, G. Rigo, and P. Sesma, “The two scales of new physics in Higgs couplings,” *JHEP* **08** (2023) 019, [arXiv:2305.19325 \[hep-ph\]](#).
- [19] M. E. Peskin and T. Takeuchi, “A New constraint on a strongly interacting Higgs sector,” *Phys. Rev. Lett.* **65** (1990) 964–967.
- [20] M. E. Peskin and T. Takeuchi, “Estimation of oblique electroweak corrections,” *Phys. Rev. D* **46** (1992) 381–409.
- [21] Gfitter, “Constraints on the oblique parameters and related theories.” http://project-gfitter.web.cern.ch/project-gfitter/Oblique_Parameters/.
- [22] L. Di Luzio, R. Gröber, and G. Panico, “Probing new electroweak states via precision measurements at the LHC and future colliders,” *JHEP* **01** (2019) 011, [arXiv:1810.10993 \[hep-ph\]](#).
- [23] **ATLAS** Collaboration, G. Aad *et al.*, “Combined measurements of Higgs boson production and decay using up to 80 fb^{-1} of proton-proton collision data at $\sqrt{s} = 13 \text{ TeV}$ collected with the ATLAS experiment,” *Phys. Rev. D* **101** no. 1, (2020) 012002, [arXiv:1909.02845 \[hep-ex\]](#).
- [24] **ATLAS** Collaboration, G. Aad *et al.*, “Search for heavy long-lived multi-charged particles in the full LHC Run 2 pp collision data at $\sqrt{s} = 13 \text{ TeV}$ using the ATLAS detector,” [arXiv:2303.13613 \[hep-ex\]](#).
- [25] L. Di Luzio, R. Gröber, J. F. Kamenik, and M. Nardecchia, “Accidental matter at the LHC,” *JHEP* **07** (2015) 074, [arXiv:1504.00359 \[hep-ph\]](#).
- [26] **CMS** Collaboration, V. Khachatryan *et al.*, “Search for long-lived charged particles in proton-proton collisions at $\sqrt{s} = 13 \text{ TeV}$,” *Phys. Rev. D* **94** no. 11, (2016) 112004, [arXiv:1609.08382 \[hep-ex\]](#).
- [27] **ATLAS** Collaboration, M. Aaboud *et al.*, “Search for doubly charged Higgs boson production in multi-lepton final states with the ATLAS detector using proton–proton collisions at $\sqrt{s} = 13 \text{ TeV}$,” *Eur. Phys. J. C* **78** no. 3, (2018) 199, [arXiv:1710.09748 \[hep-ex\]](#).
- [28] A. Alloul, N. D. Christensen, C. Degrande, C. Duhr, and B. Fuks, “FeynRules 2.0 - A complete toolbox for tree-level phenomenology,” *Comput. Phys. Commun.* **185** (2014) 2250–2300, [arXiv:1310.1921 \[hep-ph\]](#).
- [29] C. Degrande, C. Duhr, B. Fuks, D. Grellscheid, O. Mattelaer, and T. Reiter, “UFO - The Universal FeynRules Output,” *Comput. Phys. Commun.* **183** (2012) 1201–1214, [arXiv:1108.2040 \[hep-ph\]](#).

- [30] J. Alwall, R. Frederix, S. Frixione, V. Hirschi, F. Maltoni, O. Mattelaer, H. S. Shao, T. Stelzer, P. Torrielli, and M. Zaro, “The automated computation of tree-level and next-to-leading order differential cross sections, and their matching to parton shower simulations,” *JHEP* **07** (2014) 079, [arXiv:1405.0301 \[hep-ph\]](#).
- [31] A. L. Read, “Modified frequentist analysis of search results (The CL(s) method),” in *Workshop on Confidence Limits*, pp. 81–101. 8, 2000.
- [32] A. L. Read, “Presentation of search results: The CL_s technique,” *J. Phys. G* **28** (2002) 2693–2704.
- [33] L. Allwicher, P. Arnan, D. Barducci, and M. Nardecchia, “Perturbative unitarity constraints on generic Yukawa interactions,” *JHEP* **10** (2021) 129, [arXiv:2108.00013 \[hep-ph\]](#).
- [34] L. Di Luzio, J. F. Kamenik, and M. Nardecchia, “Implications of perturbative unitarity for scalar di-boson resonance searches at LHC,” *Eur. Phys. J. C* **77** no. 1, (2017) 30, [arXiv:1604.05746 \[hep-ph\]](#).
- [35] D. Barducci, M. Nardecchia, and C. Toni, “Perturbative unitarity constraints on generic vector interactions,” *JHEP* **09** (2023) 134, [arXiv:2306.11533 \[hep-ph\]](#).
- [36] M. Cepeda *et al.*, “Report from Working Group 2: Higgs Physics at the HL-LHC and HE-LHC,” *CERN Yellow Rep. Monogr.* **7** (2019) 221–584, [arXiv:1902.00134 \[hep-ph\]](#).
- [37] E. Witten, “An SU(2) Anomaly,” *Phys. Lett. B* **117** (1982) 324–328.